UNIVERSITÀ DEGLI STUDI DEL PIEMONTE ORIENTALE

"AMEDEO AVOGADRO"

DIPARTIMENTO DI SCIENZE DEL FARMACO

Corso di Laurea Magistrale in Biotecnologie Farmaceutiche

TESI DI LAUREA

GLOWING UP SOLID LIPID NANOPARTICLES: DEVELOPMENT, CHARACTERIZATION AND INCORPORATION OF FLUORESCENT DYES

Relatore

Prof.ssa Ivana Miletto

Candidato

Alessia Ialeggio

Correlatori

Dott.ssa Simona Sapino
Dr. Enrico Greco

Firmato digitalmente da Ivana Miletto
Data: 26.09.2025 10:21:49 CEST
Organizzazione: UNIVERSITA' DEGLI STUDI DEL PIEMONTE ORIENTALE/01943490027

Sessione Autunnale

Anno Accademico 2024-25

Just keep swimming

1. INTRODUCTION 7

1.1. SOLID LIPID NANOPARTICLES (SLN) 7
1.1.1. Nanoparticulate systems 7
1.1.2. Lipidic nanocarriers formulation 9
1.1.2.1. Preparation methods for lipid NPs 11
1.1.3. SLNs main applications 12

1.2. CYANINE DYES 14
1.2.1. Fluorescent dyes 14
1.2.2. Cyanine structure 16
1.2.3. Main applications 18

1.3. THERANOSTIC 20

2. AIM 23

3. MATERIALS AND METHODS 24

3.1. MATERIALS 24

3.2. METHODS 25
3.2.1. Synthesis of 3-octyl-(1,1,2-trimetil-1H-benzo[e]indol-3-io) [AI1] 25
3.2.2. Synthesis of [AI2] 26
3.2.3. Physicochemical characterization of AI 2 compound 27
3.2.3.1. Determination of molar absorption coefficient (ε) 27
3.2.3.2. Determination of quantum yield using fluorescence spectroscopy 28
3.2.4. Solid Lipid Nanoparticles (SLNs) preparation 29
3.2.4.1. Blank SLNs formulation 29
3.2.4.2. Cyanine dye-SLNs formulation 31
3.2.4.3. CURC-Cy3 SLNs formulation 32
3.2.5. SLNs purification 32
3.2.5.1. Gel filtration (GF) 32
3.2.5.2. Dialysis 33
3.2.6. SLNs characterization 34
3.2.6.1. Determination of mean diameter using DLS 35
3.2.6.2. Determination of Zeta potential 35
3.2.6.3. Observation by fluorescence microscopy 37
3.2.6.4. Entrapment efficacy 37
3.2.7. SLNs fluorescence characterization 37
3.2.7.1. FRET test 38
3.2.8. HPLC-RP chromatographic analysis 39
3.2.8.1. HPLC analysis of Cy3 39
3.2.8.2. HPLC analysis of CURC 40
3.2.9. In vitro release test 41

4. RESULTS AND DISCUSSION 43

4.1. IODOCTYL-SUBSTITUTED BENZOINDOLE CYANINE DYE 43
4.1.1. Structure 43

4.1.2. Synthesis 44
4.1.3. Spectrophotometric properties 45
4.1.4. Spectrofluorimetric properties 47

4.2. PREPARATION AND CHARACTERIZATION OF SLN 49
4.2.1. Determination of mean diameter using Dynamic Light Scattering (DLS) 51
4.2.2. Determination of zeta potential 52

4.3. ENTRAPMENT EFFICIENCY EVALUATION 54
4.3.1. Quantification by HPLC 54
4.3.2. Observation by fluorescence microscopy 55

4.4. SLN FLUORESCENCE CHARACTERIZATION 55
4.4.1. FRET analysis 57

4.5. IN VITRO RELEASE TEST 61

5. CONCLUSIONS 63

6. BIBLIOGRAPHY 64

1. INTRODUCTION

1.1. SOLID LIPID NANOPARTICLES (SLN)

1.1.1. Nanoparticulate systems

The concept of nanotechnology was first introduced in the 1970s, but it was during the 1980-90s that it began to develop significantly, driven by the advances of materials science and technology. Nanotechnologies have now applications in a wide range of fields, from medicine and materials science to energy and electronics.

Nanomaterials, as defined by EU directives, are materials with structural components in the nanoscale range (between 1 and 100 nm, 1 nm corresponds to 10^{-9} m). They are classified as nano-objects when at least 50% of the total objects have at least one of their dimensions in nanometric scale, as measured by Nanoparticle Tracking Analysis (NTA). Nanomaterials may be considered nanostructured when their internal or external surfaces are in nanoscale.

Due to their dimensions, nanosystems exhibit physicochemical properties intermediate between isolated molecules and macroscopic systems. Particularly useful in medical applications is their extremely high surface to volume ratio which allows for increased drug loading and release. Nevertheless, the high surface area, combined with the hydrophobicity of certain nanoparticles, enhance particles opsonization and degradation reducing their circulation time in vivo.[1]

Restricting our overview to nanosystems for drug delivery and nanomedicine for advanced therapies, nanoparticles of various types can be identified. Nanoparticles (NPs) have all three dimensions in nanoscale that are not significantly different in size; they are mainly classified according to the material used for their synthesis: organic and bio-inspired (proteins, carbohydrates, lipids, viral), synthetic and inorganic.[2]

- Organic and bio-inspired

  These are biodegradable and generally non-toxic NPs, due to their biological nature they are sensitive to heat and light. Apart from dendrimers, most of these NPs are based on self-assembly, generating a dynamic system that can fuse together or reorganize. However, sizes may sometimes exceed 100 nm and the truly nanometric definition.[3]

  - Liposomes – formed by self-assembly of phospholipids in a bilayer, their size may be controlled by surfactant length and range from 20 nm to several micrometers. They can encapsulate hydrophilic drugs in the aqueous core and hydrophobic drugs in the lipid bilayer; the loading capacity may be increased by

synthetizing multilamellar liposomes. Functionalization and targeting can be achieved by conjugating specific ligands or polyethylene glycol (PEG) chain to avoid reticuloendothelial system (RES) and increase their lifespan.

  - Solid-Lipid Nanoparticle (SLN) – the solid-lipid core is stabilized by surfactants allowing for hydrophobic drug loading.
  - Nanobubbles – these consist of a protein or lipid shell filled by air or nitrogen. Their surface may be functionalized with PEG or other targeting ligands, drugs may be conjugated or encapsulated. These theranostic systems combine drug delivery with ultrasound imaging since the gas core provides high contrast for this imaging technique.

- Synthetic
  - Polymeric – structures made from natural or synthetic polymers such as polylactic acid (PLA), poly(lactic-co-glycolic acid) (PLGA) or chitosan. Widely used in drug delivery, imaging, and diagnostics since they can be engineered to be biocompatible, biodegradable and capable of controlled release of drugs. Dendrimers are a subtype of polymeric NPs: they are branched and iterative polymers forming a single molecule with variable size, even below 10 nm. They may be functionalized and loaded with drugs either through covalent bonds or physical adsorption.
  - Micelles – self-assembly of amphiphilic molecules (e.g. phospholipids, surfactants) in a monolayer that in aqueous environment allows the loading of hydrophobic drugs.
- Inorganic

  Typically composed of only carbon atoms, metals and ceramics. Their composition allows for unique thermal and magnetic properties that enables applications in imaging, photodynamic or photomagnetic therapies.
  - Carbon-based – nanotubes and nanofibers are used as structural reinforcement due to their strength, while spherical nanomaterials (fullerenes) find applications in drug delivery and advanced therapies.
  - Metal-based – silver (Ag) and gold (Au) nanoparticles and several metal oxides such as iron oxide (Fe_3O_4), zinc oxide (ZnO) are widely used in imaging, drug delivery and especially photothermal therapy thanks to their excellent antibacterial and thermal properties.

- Ceramic-based – include nonmetallic solids constituted for example by silica (SiO_2) or hydroxyapatite (HA), the structure may be dense or porous to load higher quantity of drug or dye.[4]
- Quantum Dots (QD) – semiconductor nanocrystals, generally of toxic elements such as cadmium (Cd) and lead (Pb), their fluorescence is dependent on particle size and are mainly used for cells and molecules labelling and tracking.

- Nanocomposites / biohybrids

  These are hybrid nanostructures that combine materials of different nature to achieve enhanced functional properties. Nanocomposites typically combine organic and inorganic components, such as metal, ceramic or polymers. Biohybrids integrate biological elements (proteins, antibodies, DNA) with nanoscale materials for biomedical or diagnostic applications.

1.1.2. Lipidic nanocarriers formulation

Lipid-base nanostructures, including liposomes, SLNs and Nanostructured Lipid Carriers (NLCs), are generally biodegradable and biocompatible. They can encapsulate both hydrophilic and lipophilic compounds, protecting them from chemical and enzymatic degradation; although their physical stability can vary depending on the formulation.
Lipidic carriers can improve the biodistribution of drugs and modulate their pharmacokinetic properties thus enhancing therapeutic effect and minimizing adverse side effects. Thanks to their lipophilic nature, lipid NPs show advantages for clinical administration as they generally exhibit high skin compatibility and can improve drug delivery across biological barriers, such as stratum corneum of the skin and, with appropriate modifications, the blood-brain-barrier.
However, formulation studies are essential to investigate the drug – lipids – surfactants interactions, as well as their mechanisms of encapsulation and release profiles to optimize performance.[5]

Since nanoscale lies between bulk materials and isolated molecules, two opposite synthetic strategies may be applied and integrated. Top-down approaches are based on miniaturization of materials produced at microscale whereas bottom-up approaches construct nanosystems through molecular self-assembly.[1]

Liposomes, naturally occurring in organisms, are artificially engineered as vesicular delivery systems for pharmaceutical use and drug delivery. Their phospholipid bilayer specifically interacts with biological membranes enhancing biocompatibility and cellular uptake. However, liposomes often display limited stability and thus a short lifespan, they can also encapsulate, at low efficiency, mainly hydrophilic drugs.
Liposome preparation typically involves dissolving lipids in an organic solvent, removing it to form a thin lipid film, dispersing the film in an aqueous phase to produce vesicles and reducing their size by methods such as extrusion or sonication. A purification step may be carried out to remove unencapsulated material or residual solvent.

Emulsions are liquid heterogeneous systems in which a continuous, external, phase and an internal phase are stabilized by surfactants. In an oil-in-water (O/W) emulsion, hydrophobic substance (oil) droplets are dispersed in an aqueous continuous phase.
Microemulsion (μEs) are related systems that are monodispersed, thermodynamically stable, transparent and composed of nanometer-sized droplets (1 – 100 nm). Typically they form spontaneously upon mixing suitable proportion lipids, surfactants, co-surfactants and water.
μEs, being stable systems with very small droplets size, are mainly used as drug delivery systems to improve solubility and bioavailability of drugs.

Building on these concepts, in the early 1990s lipid nanoparticles emerged as a response to the limitations of conventional colloidal carriers such as emulsions, liposomes and polymeric nanoparticles. Researchers were searching for a system that combined the advantages of these carriers –biocompatibility, protection of sensitive molecules, controlled release– with improved physical stability and lower toxicity. Nevertheless, their surface can be extensively modified to enable site specific targeting and controlled drug release.

SLNs are a first-generation of lipid NPs characterized by a solid lipid core stabilized by surfactants, in which lipophilic drugs can be encapsulated. SLNs offer several specific advantages over other lipidic NPs, including their low risk of biotoxicity, the ability to induce EPR effect and the minimal to no use of organic solvents during synthesis. However, they also present some limitations, such as relatively low drug loading capacity and the risk of burst effect, that is an uncontrolled release of drug within the first hours of administration.

To address these drawbacks, NLCs were developed as the second generation of lipid NPs. Unlike SLNs, NLCs incorporate a mixture of solid and liquid lipids in the core, which creates structural imperfections in the lipid matrix. This design is associated with increased drug loading capacity, improved long-term stability and reduced risks of premature drug leakage or uncontrolled release.[5]

1.1.2.1. Preparation methods for lipid NPs

A brief overview of principal lipidic NPs preparation methods is presented below.
High pressure homogenization consists in a mixture of lipids, surfactants, water and drugs forced at high pressure through very small tubes to fragment particles into nanometric size, the process is repeated in multiple cycles. This method has been used for many years for its short production time and easy scalability. However, a main drawback is the high temperature reached in hot homogenization that interferes with heat-sensitive compounds.
Solvent emulsification and diffusion technique is based on the production of an O/W emulsion in which the organic solvent of lipids is partially miscible with water, this allows for solvent diffusion in water when the latter is added leading to the precipitation of SLNs.
Less common methods include prolonged sonication and subsequent cooling of a hot emulsion to reduce droplets size and phase reversal technique by mixing components at high temperature followed by cold dilution with water to form NPs. [5]

The µE method is widely used, the µE is prepared by melting lipids and heating the aqueous phase and surfactants to the same temperature, the µE is then dispersed in cold water to obtain SLNs.[6] This major drawback is the high temperature required, above the lipid melting point, which may damage the active compounds.
The µE method issue of temperature is overcome by the application of *cold dilution of µE* method, its main difference relies on the lower temperature used throughout the process.
This technique involves the preparation of an O/W µE where the internal oil phase consists of a solution of solid lipid solubilized in a partially water miscible solvent at moderate temperature. Both solvent and the external phase, water, are mutually saturated at room temperature to ensure the initial thermodynamic equilibrium before use in µE formulation.

To obtain the SLNs suspension the μE is diluted with cold water, this allows the solvent of the internal phase to diffuse in the aqueous phase due to its affinity for water thus precipitating the lipid as nanoparticles. [7]
The SLNs thus obtained generally have two main drawbacks: the high concentrations of surfactants used relative to the lipid phase and the strong dilution of the final SLNs suspension.

1.1.3. SLNs main applications

SLNs find applications in pharmaceutical and medicine, as well as in the food and cosmetic industries.
An advantage of using these nanocarriers is their easy and cheap production process, which can be easily upscaled.
Nanometric dimensions, in contrast to microscale systems, enable intracellular targeting. Cells, typically in the range of tens of micrometers, are generally unable to internalize microparticles larger than 1 μm. These small dimensions also allow parenteral injections as well as oral, topical or ocular administration.
Their application as drug delivery systems is linked to their ability to enable controlled drug release and to increase lipophilic drug bioavailability.

Their wide use as molecule carriers is supported by their biocompatibility and lipophilicity. These characteristics give SLNs, unlike free drugs, the ability to cross otherwise difficult biological barriers such as blood-brain and ocular. Blood-brain barrier is a physical and enzymatic barrier that isolates neural tissue from bloodstream to protect it, while drug delivery to the eye is limited by the cornea, sclera and retina. SLNs can overcome these barriers and deliver drugs, proteins, antibodies and contrast substances for imaging to both the brain and the eye, to the anterior part by topical administration and to the posterior part by injection.
Chemotherapeutics generally have poor solubility in water, bioavailability, therapeutic index and delivery to cells. SLNs offer the possibility to bind specific ligands to the nanoparticle surface to enable site-specific targeted drug delivery. This strategy allows specific binding to the appropriate receptors on cancerous cells, followed by release of the chemotherapeutic drug into the cells. This mechanism increases drug delivery and efficacy.
Incorporation of proteins or peptides inside SLNs has allowed their efficient delivery to the target while enhancing their stability. Examples of entrapped polypeptides are insulin,

somatostatin and calcitonin. Antigens can also be delivered, making SLNs efficient and safe non-viral vectors for vaccines thanks to the absence of proteins and therefore of immunogenicity. Vaccines based on DNA, RNA and mRNA can also be administered using SLNs, which protect the fragile mRNA from extracellular degradation.
SLNs are also used in the food industry, for example for oral administration of lipophilic, insoluble and unstable dietary supplements such as carotenoids.[5]

A different therapeutic approach, compared to drug delivery, is photodynamic therapy (PDT), which relies on a photosensitizer molecule to generate ROS and selectively kill target cells. Photosensitizers are often lipophilic metallic compounds with poor bioavailability and low solubility in aqueous media, making their encapsulation in SLNs particularly advantageous combined with the nanoparticles improved skin penetration and safety. This strategy has been investigated by encapsulating aluminum chloride phthalocyanine in SLNs for use in topical melanoma formulations to enable PDT.[8]
SLNs can be used in biological imaging: MRI, SPECT or optical imaging is used applying different probes. Studies inserting fluorescent probes, such as Nile Red, in the lipidic core have been conducted to study the cellular uptake and applicability of the model, having the dye mimicking a therapeutic payload.[9] To investigate the intracellular localization of SLNs is necessary to have a dye that do not suffer form release from SLNs matrix. Kristl et al. have created a personalized coumarin-derivative containing a long lipophilic chain that allows incorporation on nanoparticle surface. This study said that the majority of SLNs localized in the perinuclear region, common to other NPs, some SLNs also show association with actin filaments, mitochondria. There is no co-localization with lysotracker, an indicator that SLNs may be degraded through other mechanisms.[10]

An advancement of both drug delivery and imaging systems has led to the development of theranostic system, lipidic NPs are particularly appreciated in this application over other nanoparticles mainly for their biocompatibility and safety. Metals or inorganic agents can be inserted as MRI contrast agents as well as fluorophores for optical imaging. This application for SLNs is however still mainly unexplored and more studies need to be conducted.[11]
For example, SLNs-based theranostic can be used to treat rheumatoid arthritis by combining methotrexate, an anti-inflammatory drug, a monoclonal antibody against the macrophage-

specific receptor CD64 (overexpressed in rheumatoid arthritis) and superparamagnetic iron oxide used as an MRI contrast agent.[12]

1.2. CYANINE DYES

1.2.1. Fluorescent dyes

Fluorescence is a radiative process in which the energy of an excited molecule is released as electromagnetic radiation.

According to Jablonsky scheme, electrons in atoms are arranged in electronic energy levels, the population of these levels follows Boltzmann distribution, which can simplified as

$$\frac{N_1}{N_0} = e^{\left(\frac{-\Delta E}{kT}\right)} \quad (1)$$

where N_1 and N_0 are the populations of an excited and ground electronic level, ΔE is the energy difference between the two levels, k is Boltzmann constant, T is temperature.

It can be assumed that at room temperature all electrons are virtually placed in the lowest possible electronic level S_0 (ground state).

When a molecule absorbs a high energy photon, typically in the UV-Vis range, one electron is promoted to an excited and unstable energetic level from which it subsequentially decays.

Fluorescence decay times are in the range of 10^{-10} – 10^{-7} seconds, thus competing with non radiative decays such as inter-system crossing and or internal conversion, vibrational relaxation, which occur on faster timescales. During vibrational relaxation part of the energy is dissipated before fluorescence emission takes place. In addition, excited molecules have a different dipole moment than in the ground state, causing the solvent to reorganize around the molecules toward a new equilibrium configuration. This rearrangement occurs in timescales slower than absorption but faster than fluorescence emission, stabilizing the excited molecule at a lower energy.

Vibrational and solvent relaxation together explain why the maximum of fluorescence emission occurs at longer wavelengths (lower energy) than the absorption maximum. This shift, called Stokes shift, is characteristic of each fluorophore, larger Stokes shifts are preferred to avoid effects such as re-absorption of emitted light that generate background noise.

A dye is a molecule that exhibits strong absorption in the visible portion of the electromagnetic spectrum thus giving bright color to its solution, a fluorescent dye can re-emit part of the absorbed energy as fluorescence, acting as a fluorophore.[13]
An organic fluorophore can absorb radiation due to the delocalization of electrons along its structure.
The structural features that are necessary, but not sufficient, for a fluorophore include a rigid conjugated π-system (e.g. vinyl groups in a chain or aromatic rings, often fused together to increase rigidity) and the presence of an electron donating group (EDG) and an electron withdrawing group (EWG).

Ideal fluorophores to be used as probes for biological optical imaging should have high molar absorption coefficient to efficiently absorb radiation, high quantum yield (close to 1), emission in the red region to limit tissue autofluorescence and damage, resistance to photobleaching, no toxicity.

Synthetic fluorophores used in biological applications can be divided into classes based on their structure. The four most common classes of commercial fluorescent dyes are coumarins, xanthenes, BODIPYs and cyanines.[14]

- Coumarins are natural secondary metabolites of various plants and microorganisms, their core scaffold is a benzo-α-pyrone with a phenol or amine substituent in position 7 which allows their use as fluorophores. The extended π-conjugated system of these compounds is responsible for their fluorescent properties, and the base structure can be widely modified. The conjugated system can be further enhanced by introducing EWG on position 4 and EDG in position 6 and 7 or by fusion with additional rings such as furan, pyran, phenyl moieties, these modifications red-shift coumarins emission. Articles report encapsulation of coumarins inside different types of nanoparticles to label them but their main application as fluorescent probes is for the identification of ions and small molecules in complex matrices such as water and biological systems.[15][16]
- Xanthenes are natural secondary metabolites of plants, like coumarins, whose core structure is a tricyclic xanthene scaffold, derived from anthracene. Hydroxy-xanthenes, presenting an oxygen atom bridging in position 10, are chemically modified to generate fluorescein and rhodamine, two widespread synthetic commercial dyes. Further

substitutions with benzoic acid in position 9 and with amino, carbonyl or hydroxyl groups in position 3 and 6, which can be protonated, introduce EWG and EDG. This scaffold may be modified to induce red-shift of emission, this is achieved by substitution of EDG auxochromes, or by addition of EWG achieved by switching heteroatom in position 10 or by halogenations, however the emission is not easily tunable maintaining high yields.[17]

- BODIPY (boron dipyrromethene) is a class of entirely synthetic fluorophores that exhibits many of the characteristics of ideal fluorophores and can be easily modified to produce derivatives with different properties. The core structure consists of two pyrrole rings connected through a methine bridge, pyrrole nitrogens coordinate a boron substituted by two fluorine atoms, the electron-deficient boron and the electron-rich pyrrole nitrogens together constitute the intrinsic EDG-EWG system. The emission can be red-shifted by substitutions along the structure, however precise mechanisms of BODIPY emission tuning are not clearly understood yet. More complex systems may be obtained by substituting strong EWG or EDG in meso-position, allowing the entire BODIPY core to behave as an electron donor or acceptor based on the substitution. Their main application is in ions detection and in photodynamic therapy (upon irradiation, dyes allow both fluorescence imaging and reactive oxygen species (ROS) generation leading to apoptotic cell death), BODIPY can be encapsulated inside nanoparticle however significant leakage is observed unless the dye is functionalized with long alkyl chain.[18][19]

1.2.2. Cyanine structure

Cyanines are a class of fluorescent dyes especially used as optical imaging probes.
Their core structure consists of two polycyclic aromatic groups (typically indoles) linked by a polymethine bridge, the two indole nitrogens are part of a π-conjugated system.
To have fluorescent properties both nitrogens are substituted with R groups to obtain quaternary nitrogen. The quaternized nitrogens can alternatively gain a positive charge due to electron delocalization through the indoles and the methine bridge, the positive charged moiety (N^+-R) functions as the electron withdrawing group while the nitrogen on the other indole will serve as the electron donor group.

Key feature of cyanine dyes is that wavelength of absorption and emission depends on the length of the polymethine bridge, as the methine units (-CH=) increase, the emission shifts of approximately 100 nm to longer wavelengths.

- Monomethine cyanine dyes have a single methine group bridging the terminal groups that confers absorption and emission in the 450-470 nm range. Their main application is in nucleic acid labeling, however due to the short-conjugated system their brightness is lower than other cyanine.
- Trimethine cyanine dyes absorb and emit efficiently in the 550-570 nm range. Their visible-range emission allows application in biological cells and organisms imaging and in cellular and molecular assays such as Fluorescent In-Situ Hybridization (FISH), Polymerase Chain Reaction (PCR) and flow cytometry.
- Pentamethine cyanine dyes have emission shifted to the far-red region (650-670 nm range). This range allows for in vivo and in vitro biological applications in microscopy and labeling, while maintaining good stability of dye.
- Heptamethine have a seven-carbon bridge and exhibit emission in the near-infrared (NIR) region with absorption peak around 750 nm and emission around 780 nm or higher. This range is optimal for deep-tissue biological imaging; however it comes with decreased photostability due to photooxidation and photoisomerization (light-induced trans-cis isomerization around the polymethine bridge), this issue is reduced by making the chain more rigid to minimize bridge flexibility.[20]

Various substituents may be added to the polymethine bridge to tune dye emission, they can be small groups, halogens or fused rings to rigidify the chain and improve stability.
Dewar theorized a set of rules to predict the effect of substituting electron donating or withdrawing groups into the conjugated system, this is useful for rational design of cyanine dyes since the same substituent may have opposite effect on emission based on its position. Substituting a EWG or introducing a heteroatom in a *starred* position induces a hypsochromic shift (blue-shift) or a bathochromic shift (red-shift) when in an *unstarred* position and vice versa for EDG substitution.[21]

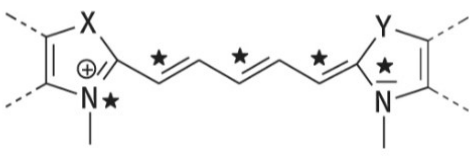


Figure 1.1 - Dewar's rule illustration[21]

Starred positions correspond to odd positions in the polymethine bridge. For instance, addition of EDG such as fluorine or methoxy group (OMe) in position 3 gives a red-shift whereas iodine or bromine act as EWG inducing instead a blue-shift.

Cyanine dyes are highly customizable dye, not only along the polymethine bridge, but also substituents of the terminal rings and of the nitrogens may be extensively modified to confer respectively different photophysical and solubility properties to the dye.
Sulfonate groups (SO_3^-) increase cyanine polarity and solubility in water when substituted on nitrogen or on the indoles, their presence also introduces electrostatic repulsion between molecules reducing stacking effect and resulting in bathochromic shifts of emission.[22]
Alkyl chains of various lengths further enhance cyanine lipophilicity without affecting wavelengths of absorption and emission.[23]
One or more benzene rings can be fused to the indoles forming benzo[e]indole to red-shift emission, even longer shifts may be obtained by alternative ring fusion to generate a benzo[c,d]indole. These effects are due to the enhancement of conjugation on terminal groups.[24]

1.2.3. Main applications

In the early years of technology, before becoming widespread tools in biological imaging, cyanine dyes found broad application in optical data storage systems thanks to their ability to interact with visible and near-infrared light sensitizing various materials. From silver halide coatings in photographic plates to coating of compact discs (CDs) to render them recordable, all the way to modern offset lithography by coating the heat sensitive plates with NIR-sensitive cyanine dyes which can convert laser rays to heat to produce the image on the plate.

Cyanine dyes, thanks to their versatile possibilities of structural modification, are especially used as fluorescent markers for small molecules identification and for biological labeling and imaging, the dye can interact with a substrate to form a complex both covalently and not.

- Non-covalent protein labeling – cyanine dye is introduced as aqueous solution in living organisms to detect proteins to which they can bind non specifically. Water-soluble dyes

are needed, such as cyanine modified with sulfonate groups or the commercially available Indocyanine Green (ICG).

- Covalent protein labeling – a reactive group is attached to the cyanine through a spacer, this group (e.g. maleimide for cysteine or methionine residues) can selectively react with the target protein through various mechanisms. The most precise labeling can be achieved using click chemistry, which employs only non-natural functional groups to react and avoid any off target.
- Non-covalent DNA labeling – intercalation occurs when a molecule inserts itself between DNA base pairs, fluorescent dyes that intercalate allow DNA imaging. Cyanine dyes designed to intercalate DNA have an additional positive charge, such as a third quaternized nitrogen, to have stronger interactions thanks to electrostatic attraction.
- Covalent DNA labeling – a phosphoramidite group can be attached to the dye to react with the free -OH at 5'-end of an oligonucleotide and selectively label it. This is used in DNA sequencing as a safer alternative to radioactive labeling.[21]
- ROS sensing – the C2-N bond of the indole ring can be reduced to form a hydrocyanine, ROS quickly oxidize the bond, restoring the conjugated system and thus cyanine fluorescence. ROS levels are monitored since they are often elevated under oxidative stress and in tumor cells.
- pH sensing – cyanines with unsubstituted indole nitrogen can become fluorescent in acidic environments upon nitrogen protonation. Alternatively, cyanines functionalized with piperidine derivatives on the polymethine chain can shift wavelength of absorption after protonation allowing ratiometric sensing. Detecting lower pH values is useful in tumor identification.
- Thiol sensing – thiols such as cysteine and glutathione may be dysregulated in pathology. Thiol can react with cyanines by performing a Michael addition to eliminate an ester substituent causing a blue-shift in emission and allowing ratiometric monitoring, alternatively they can reduce a disulfide bond thus releasing the dye from a pro-drug to have theranostic effect.[25]
- Fluorescence-guided surgery – water-soluble dyes, such as ICG, can bind to albumin and therefore circulate in the bloodstream, making it visible for angiography via NIR imaging to visualize tissue perfusion, anatomical structures and lymphatic system. [26]
- Medical diagnostic – ICG is, to date, the only FDA approved dye for direct administration, it can be used as a fluorescent or NIR absorption agent. [27]

Cyanine dyes are often entrapped into nanoparticles to enhance their performance in both in vitro and in vivo applications. Entrapment leads to the creation of theranostic nanosystems that combine advantages of nanocarriers, such as elevated cellular uptake and low toxicity, with improved dye characteristics, as increased photostability and water solubility. These systems are effective in drug delivery and, through targeting strategies, offer low invasive detection of tumor location and development.

Targeted nanoparticles are frequently employed to increase therapeutic activity in the desired target. For example, a chitosan coating provides mucoadhesive properties for application in breast cancer cells, while functionalization with epidermal growth factor receptor ligands can direct nanoparticles to colorectal cancer cells.

When a dye and an anticancer drug are co-encapsulated the resulting system may exhibit a trivalent mechanism of action. The nanoparticle allows for a sustained release of drug inside the cellular environment, while the dye can be exploited for both photodynamic therapy, leading to ROS generation and cell death, and tumor imaging.

Nanosystems may also take advantage of high retention effects and enhanced permeability (EPR effect) that promotes nanoparticle accumulation in tumors improving imaging sensitivity.

It is important to evaluate not only the system stability but also its biodistribution in the organism to avoid excessive retention or off-target effects. For instance, ICG can increase nanoparticles affinity to plasma proteins, improving biodistribution but also inducing fluorophore leakage.[28]

1.3. THERANOSTIC

Nanotherapeutic applications in cancer treatment have proven successful in increasing chemotherapeutic solubility and biodistribution; however, these approaches have not been shown to be completely effective. In a study conducted by Harrington et al.[8], the tumor uptake of PEGylated liposomes was monitored, confirming that EPR effect alone does not guarantee sufficient drug concentration in tumor cells for every patient and under every condition. This is mainly due to tumor heterogenicity and the various obstacles that the tumor microenvironment poses to NPs diffusion.

It is increasingly clear that tumor diagnosis plays a crucial role in the precise administration of chemotherapeutics: tumor extension, developmental stage and abnormalities identified through diagnostic imaging are essential to determine the most effective therapeutic strategy.
It is within this perspective that theranostic emerges: it is defined as the combination of therapy and diagnosis, where both drugs and imaging probe are co-administered -often within a single nanoparticle- to achieve simultaneous treatment and monitoring.
This approach allows real-time tracking of treatment progress and cancer development, as well as gathering information on drug pharmacokinetic such as the amount of drug that reaches tumor cells, the amount of released drug and any off-site distribution.

Lipid nanoparticles (LNs) are preferred in theranostic approaches mainly thanks to their elevated biocompatibility and safety. They also offer other advantages such as targeting possibilities, elevated half-life in vivo and, although different based on NPs type, a generally high encapsulation efficiency.
However, one of the major limits in developing these kinds of systems is the simultaneous incorporation of multiple compounds inside a single NP, this is a formulation problem that may result in high polydispersity and heterogeneity of sample. LNs also cannot be stored for prolonged periods of time, Carregal-Romero et al.[29] have demonstrated that once stored for nine months, although maintaining comparable physicochemical properties, PEGylated NPs had completely different distribution profiles in vivo.
Liposomes, among the other lipid nanocarriers, are extremely versatile in these applications: thanks to their aqueous core they can incorporate both hydrophilic and lipophilic drugs and contrast agents, ranging from radiolabeling with isotopes for PET imaging to gadolinium (Gd)-based agents for MRI or quantum dots and organic fluorophores for optical imaging.
In SLNs the imaging agent is intercalated in the lipid matrix, studies have been conducted inserting contrasting agents for MRI, technetium-99 (^{99m}Tc) as a probe for Single Photon Emission Computerized Tomography (SPECT) or quantum dots and other fluorophores for optical imaging.[11]

Theranostic approaches are not limited to drug-based therapy but can also be coupled with PDT after co-encapsulating a photosensitizer agent with an imaging probe. If a MRI probe is inserted, the system can also be independently activated for therapy and imaging since two different techniques are used.[11]

Translating the theranostic study in vivo is still very challenging and currently no clinical trials using SLNs for theranostic purposes are registered. Although minimized using LNs, the risk of toxicity if the theranostic agent interacts with biological tissue is still a possibility. Adsorption of proteins on the NP surface alters the biodistribution in vivo. However, the major issues lie in the formulation of an economic and reproducible synthetic process that can be translated in large scale at high yield.[30]

Indeed, very few nanoparticles, used just as imaging probe and not as a theranostic platform, have currently moved to clinical settings and no one of them is a lipidic NPs. Albumin nanocolloids radiolabeled with ^{99m}Tc are used for SPECT imaging to identify sentinel lymph nodes in various types of tumors. Superparamagnetic Iron Oxide Nanoparticles (SPIONs) are MRI contrasting agents, quite discontinued in favor of Gd-based agents, but with niche applications such as in Tumor-Associated Macrophages (TAMs) identification. Microbubbles and albumin microspheres are also approved as ultrasound contrast agents.[31]

2. AIM

This thesis has been developed to establish a reproducible, simple and cost-effective method to monitor the intracellular location of solid-lipid nanoparticle (SLNs) used as drug carriers and routinely produced in our laboratory.
Generally, fluorophores are encapsulated inside the SLN as a payload, similar to drugs. In this work, however, the aim was to stably incorporate the fluorescent dye within the lipid matrix itself, to reflect the fate of the carrier rather than that of an encapsulated molecule. For this purpose, a fluorescent cyanine dye was synthesized and used to label SLNs, enabling their intracellular tracking by fluorescence microscopy.
This project represents a formulation intended for *in vitro* studies designed to provide insight into the fate of SLNs after cellular internalization, to better understand their behavior and support the rational design of future nanocarriers.

SLNs are selected as model nanocarriers because of their biocompatibility, high stability and ability to provide controlled and sustained drug release. Their production protocols are well-established in our laboratory.
Cyanine dyes are chosen thanks to their high customizability, strong brightness, ease of production and biocompatibility.

The first objective was to establish a well-assessed and reproducible SLN formulation capable of simultaneously entrapping both the fluorescent dye and a model drug. Once optimized, these formulations were subjected to thorough physicochemical and fluorescence characterization to confirm their stability and performance. The final step, not reached within the timeframe of the present work, will involve cell tests combined with microscopy analysis to determine whether SLNs remain intact upon cellular internalization or disassemble, thus clarifying the fate of the lipid components constituting the nanoparticles.

This work was carried out in collaboration between the Physico-Chemical Laboratory of the University of Eastern Piedmont and the Innovative Pharmaceutical and Cosmetic Technology and Nanotechnology (i-PHARCOTEC) Group of the University of Turin.

3. MATERIALS AND METHODS

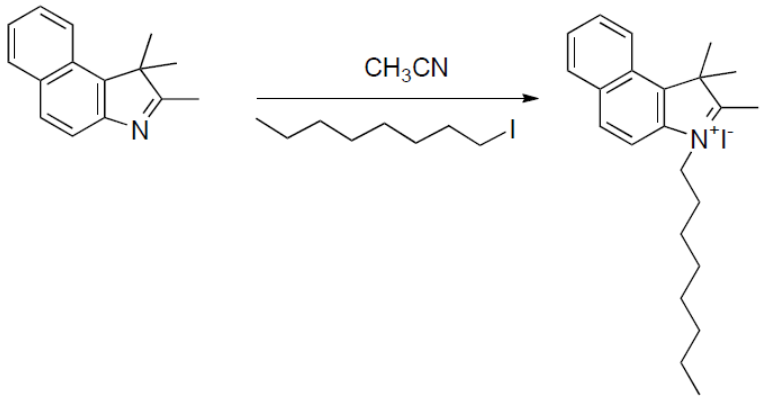
3.1. MATERIALS

Reagents were purchased from Sigma-Aldrich/Merck, BLD Pharma, Thermo-Fisher, Lucas Meyer, BASF, A.C.E.F. and used as received unless otherwise specified.
Solvents were from Fisher Scientific Italia, Carlo Erba Italia, VWR Chemicals.
Ultrapure water (18 MΩ·cm) was obtained from MilliQ® purification system by Millipore.

The physicochemical characterization of cyanine dye and of SLNs is performed using the following instruments:
NMR: Bruker Avance Neo 400 (9.4T)
MS : Ion trap spectrometer Thermo Finnigan LCQ-Deca XP-PLUS
Spectrophotometer: Shimadzu UV1900
Spectrofluorometer: Jasco FP-8650
DLS: Brookhaven Instruments Corporation, 90 Plus Particle Size Analyzer
Zetameter: Malvern Zetasizer Pro
HPLC: Younglin Co., YL9100 HPLC System
Optical microscope: Leica DM 2500
Electron microscope: Field Emission Gun Electron Microscope GeminiSEM-360 from Carl Zeiss S.p.A., Milan, Italy

3.2. METHODS

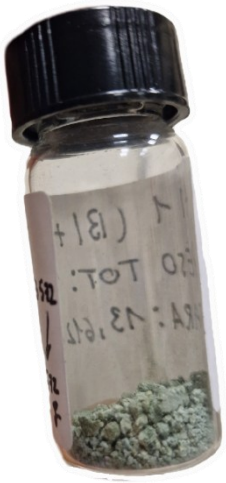
3.2.1. Synthesis of 3-octyl-(1,1,2-trimetil-1H-benzo[e]indol-3-io) [AI1]



500 mg (2.39 mmol, 1 eq) of 1,1,2-trimethyl-1H-benzo[e]indole and 1.5 mL (7.88 mmol, 3.3 eq) of iodo-octane are loaded into a round-bottom flask and dissolved in 10 mL of acetonitrile. The reaction is carried out under reflux for 20 hours in N_2 atmosphere.

Once the reaction is completed the solution is diluted in diethyl ether and the obtained solid is filtered under vacuum.

923 mg of a green solid are obtained.



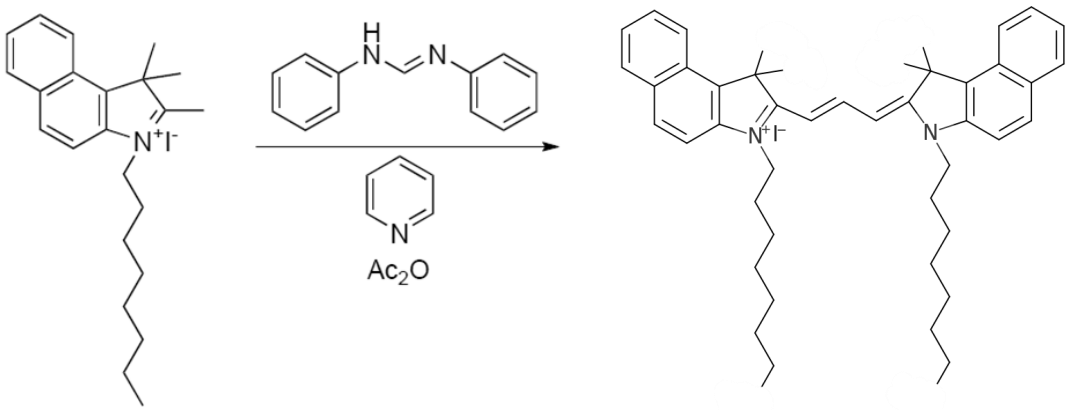
Molecular formula: $C_{23}H_{32}IN^+$

Molecular weight: 449,42 g/mol

Yield: 86.25%

^{1}H NMR: (400 MHz, MeOH d-4, 298 K) δ(ppm) 8.35 (d, 1H), 8.27 (d, 1H), 8.19 (d, 1H), 8.03 (d, 1H), 7.83 (d, 1H), 7.74 (t, 1H), 4.65 (t, 2H), 2.05 (quint, 2H), 1.87 (s, 6H), 1.61-1.3 (m, 10H), 0.91 (t, 3H)

3.2.2. Synthesis of [AI2]



500 mg (1.11 mmol, 2 eq) of compound AI1 are inserted into a round-bottom flask along with 110 mg (0.556 mmol, 1 eq) of N,N′-diphenylformamidine, 100 µL of pyridine and 10 mL of acetic anhydride.

The reaction is carried out under reflux at 140°C, under a N_2 atmosphere for approximately 4 hours, the progress of the reaction is monitored by UV-Vis absorption spectroscopy until the desired product is detected (expected λ_{abs} in 550-600 nm range).

At completion the mixture is dissolved in dichloromethane and slowly diluted in petroleum ether.

113 mg of a bronze friable solid that adhere to the vial walls are obtained.

Molecular formula: $C_{47}H_{61}IN_2$

Molecular weight: 780,92 g/mol

Yield: 26%

NMR: ^{1}H NMR: (400 MHz, MeOH d-4, 298 K) δ(ppm) 8.81 (t, 1H), 8.32 (d, 2H), 8.07 (dd, 4H), 7.71 (t, 2H), 7.66 (d, 2H), 7.55 (t, 2H), 6.54 (d, 2H), 4.31 (t, 4H), 2.13 (s, 12H), 1.93 (quint, 4H), 1.60-1.31 (m, 20H), 0.89 (t, 6H)

Exact mass: 780.39 g/mol (theorical), 653.48 g/mol ($[M-I]^-$, found)



3.2.3. Physicochemical characterization of AI 2 compound

3.2.3.1. Determination of molar absorption coefficient (ε)

Molar absorption coefficient (ε) is a measure of absorption efficiency of molecules at a given wavelength. It is an intrinsic property of chemical species and thus important for their characterization.

Lambert-Beer law relates absorbance and concentration through the following equation:

$$A = \varepsilon \cdot l \cdot c \quad (1)$$

where A is absorbance, c is concentration of the sample (mol/L), ε is molar absorption coefficient ($Lmol^{-1}cm^{-1}$) and l is path length (cm).

This equation corresponds to a straight line, concentration c is the independent variable x and $\varepsilon \cdot l$ is the slope m. Plotting absorbance versus concentration the molar absorption coefficient value can be immediately obtained as the slope of the line, given that l is fixed at 1 cm.

A stock solution of AI2 at a concentration of 10^{-3} M in dimethyl sulfoxide (DMSO) is prepared by solubilizing 3.9 mg of cyanine powder in 5 mL of DMSO.

Five standard solutions are prepared by performing serial dilution of the DMSO stock solution in 10 mL of methanol. The following concentrations are chosen:

- $C_1 = 1 \times 10^{-6}$ M
- $C_2 = 1.8 \times 10^{-6}$ M
- $C_3 = 2.5 \times 10^{-6}$ M
- $C_4 = 3.2 \times 10^{-6}$ M
- $C_5 = 4 \times 10^{-6}$ M

For each sample the absorption spectrum is recorded over a 250-700 nm wavelength range. Measurements are conducted at room temperature using a quartz cuvette with optical path length of 1 cm.

Spectra are analyzed using OriginPro software to identify the maximum absorbance value of each standard solution. These values are plotted in a -absorbance vs concentration- graph to generate the linear regression curve by interpolation, the slope of the linear regression corresponds to the molar absorbance coefficient.

3.2.3.2. Determination of quantum yield using fluorescence spectroscopy

Fluoresce emission spectra are recorded using a scan speed of 10,000 nm/min, a data interval of 1 nm, with a quartz cuvette having optical path length of 1 cm.

Quantum yield (Φ_F) is an intrinsic property of compounds; it represents the probability that an excited molecule will release photons via radiative processes over non-radiative decay. It is defined as the ratio between number of emitted photons (N_{Em}) and number of absorbed photons (N_{Abs}).

$$\Phi F = \frac{N_{Em}}{N_{Abs}} \quad (2)$$

Quantum yield of the cyanine dye was determined through comparative Williams method whose equation is used to calculate Φ_F of an unknown sample by comparison to a standard reference molecule: [32][33]

$$\Phi_s = \Phi_{std}\left(\frac{A_s}{A_{std}}\right)\left(\frac{F_{std}}{F_s}\right)\left(\frac{I_{std}}{I_s}\right)\left(\frac{\eta_s}{\eta_{s_{td}}}\right)^2 \quad (3)$$

where A is the absorbance of the sample at excitation wavelength, F is the integrated fluorescence emission intensity, I is the intensity of the exciting light and η is the refractive index of the solvent.

Since analyses of both samples are carried out in the same solvent, methanol, and using the same intensity of exciting light (same light source and same apertures), Eq. 3 can be simplified by removing the $\left(\frac{\eta_s}{\eta_{std}}\right)^2$ and $\left(\frac{I_{std}}{I_s}\right)$ terms.

By plotting absorbance (A) against integrated area of the fluorescence spectrum (F) a linear regression is obtained, and its slope (m) can be substituted to $\left(\frac{A_s}{A_{std}}\right)\left(\frac{F_{std}}{F_s}\right)$.

The resulting simplified equation is the following

$$\Phi_s = \Phi_{std}\left(\frac{m_s}{m_{std}}\right) \quad (4)$$

The reference molecule chosen should have well-definite quantum yield, it should be readily available and chemically stable, and it should have similar optical properties (such as range of absorption and emission) to that of the sample under investigation.

Rhodamine B (RhoB) is chosen as the reference, with $\Phi_F = 0.7$ [34].

RhoB stock solution is prepared at a concentration of 10^{-3} M in DMSO solubilizing 2.3 mg of RhoB powder in 5 mL of DMSO.
Five serial dilutions are prepared in 10 mL of methanol obtaining standards within the $10^{-6}/10^{-7}$ M range. This concentration range is chosen to ensure absorbance values lower than 0.3, that will guarantee the linear range of the analysis and prevents self-absorption (a phenomenon in which emitted photons are reabsorbed by sample molecules reducing apparent fluorescence). UV-Vis absorption spectra of these standards are recorded.
AI2 solutions are prepared with the same procedure and concentration range as in previous spectrophotometric analyses, and absorption spectra are acquired.
Fluorescent spectra of RhoB and AI2 solutions are registered.
RhoB samples are excited at 500 nm and emission spectra are acquired in the 520-750 nm range. AI2 solutions are excited at 550 nm, corresponding to the absorbance shoulder peak, emission spectra are acquired in the 570-750 nm wavelength range. Although the wavelength of excitation is different from that of RhoB, to obtain the maximum emission possible from each sample, the intensity of the exciting light at the two wavelengths is comparable.
Spectra are processed using OriginPro software to integrate the fluorescence emission spectra, thus obtaining the F values.

3.2.4. Solid Lipid Nanoparticles (SLNs) preparation

3.2.4.1. Blank SLNs formulation

Blank SLNs, as well as drug- and dye-loaded SLNs, are obtained using the *cold dilution of a microemulsion* technique (refer to 1.2.2.1.) which was developed in the i-PHARCOTEC laboratory of the University of Turin[7]. All SLNs in this work are prepared following previously established protocols.
This technique involves the preparation of an oil/water (O/W) microemulsion (from now on, referred as μE) employing ingredients classified as Generally Recognized As Safe (GRAS) to ensure SLNs biocompatibility and safety for biomedical applications.
The internal lipid phase of the μE consists of trilaurin (TL), the triglyceride of lauric acid, solubilized in ethyl acetate (EtOAc). Epikuron®200 (soy lecithin), Cremophor®, propylene glycol (PG) are employed as surfactants and co-surfactants. MilliQ water acts as the external continuous phase.

As a first formulation step, MilliQ water and EtOAc are mutually saturated beforehand by adding them in a separatory funnel at a 2:1 v/v ratio. The funnel is then shaken to allow mutual saturation of EtOAc and water and left 24h in vertical position to allow phase separation. Saturated water (S-water) is collected from the bottom of the funnel while the saturated EtOAc (S-EtOAc) is collected from the top of it.

The process continues with the μE preparation. Briefly, TL is solubilized in S-EtOAc under stirring and mild heating at approximately 50 °C. Once a clear solution is obtained Epikuron®200 is solubilized in it applying mild heating and stirring again, until complete dissolution. Cremophor® is added as a surfactant to obtain the internal phase of the μE, S-water is subsequently added as the continuous phase to obtain a O/W/ system. The system is then titrated by progressive additions of PG, used as a co-surfactant, in 50 mL increments, until transparency is achieved indicating the formation of a stable O/W μE.

The μE is then precipitated by adding 3ml of MilliQ water all at once under stirring to obtain a SLNs suspension.

Throughout the procedure, *mild stirring* refers to agitation in a test tube using a vortex instrument.

Composition of blank SLNs is displayed in the following table.

Table 3.1- Blank SLNs composition

Ingredients	**Quantities**
TL	60 mg
S-EtOAc)	200 μL
Epikuron®200	170 mg
Cremophor®	45 μL
S-water	700 μL
PG	100-200 μL
MilliQ water	3 mL

3.2.4.2. Cyanine dye-SLNs formulation

Starting from the blank formulation many tests were carried out to establish the most reproducible protocol aiming to obtain strong and stable cyanine dye-SLNs fluorescence signal, ease of preparation, reproducibility and an uniform and mild coloration of the final nanoparticle suspension. For the sake of clarity, AI2 cyanine dye will be hereafter referred to as Cy3.

A stock solution of Cy3 in S-EtOAc was prepared in order to improve the molecule solubility and to allow reproducible and precise incorporation of micrograms amounts of Cy3 into the microemulsion. Given the very small quantities required, direct weighing would have introduced risk of inaccuracy.
For this reason, a suitable volume of S-EtOAc have been added in a 2 mL flask to 1.6 mg of cyanine powder to obtain a $1.0 \cdot 10^{-3}$ M solution (Cy3 in S-EtOAc).

The protocol of preparation is the same used for blank SLNs with little adjustments.
TL is initially solubilized in plain S-EtOAc, then the planned amount of cyanine stock solution is added, and the procedure can progress as usual.
Four different formulations have been obtained with different volumes of cyanine stock solution, aiming to introduce increasing amounts of Cy3 ranging from 0.013% to 0.15% w/w relative to the total lipidic phase.

Table 3.2 - Cy3 SLNs composition

Components	**Quantities**			
TL	60 mg			
Sat-EtOAc	190 µL	175 µL	150 µL	100 µL
Cy3 in S-EtOAc	10 µL	25 µL	50 µL	100 µL
Epikuron®200	170 mg			
Cremophor®	45 µL			
S-water	700 µL			
PG	150 µL			
MilliQ water	3 mL			

3.2.4.3. CURC-Cy3 SLNs formulation

Curcumin (CURC), a lipophilic drug, used as a model drug loaded in the solid lipid core, is added to the formulation in powder form.
Two different formulations containing 2.5 mg and 5 mg of curcumin powder are prepared, corresponding respectively to 4% and 8% of the total lipid phase. These concentrations were previously tested in our laboratory and were known to have significant therapeutic effects and suitable release profiles.

The protocol of preparation is the same that is used for Cy3 SLNs, CURC powder is added after the solubilization of TL and Epikuron®200 in S-EtOAc.
With the same protocol, using 200 µL of plain S-EtOAc, CURC SLNs can be obtained as well.

Table 3.3 - CURC-Cy3 SLNs composition

Components	**Quantities**	
TL	60 mg	
S-EtOAc	150 µL	
Cy3 in S-EtOAc	50 µL	
Epikuron®200	170 mg	
CURC	2.5 mg	5 mg
Cremophor®	45 µL	
S-water	700 µL	
PG	150 µL	
MilliQ water	3 mL	

3.2.5. SLNs purification

3.2.5.1. Gel filtration (GF)

Initially a phosphate-buffered saline (PBS) solution (0.1 mM, pH 7.4) is prepared by adding the following salts to 2 liters of MilliQ water and keeping it under stirring until complete dissolution.
Types and quantities of employed salts are:

NaCl – 8 g

$Na_2HPO_4(H_2O)_2$ – 0.16 g

KH_2PO_4 – 0.2 g

KCl – 0.2 g

An agarose column with a length of 12 cm is prepared. Agarose beads (4% B-CL, Alfa Aesar) are poured inside the column after placing a Polyethylene (PE) Frit, 20 μm porosity filter at the bottom. Once the column is filled with agarose, at least 20 mL of PBS is introduced at the head of the column and eluted by gravity to condition it.

Gel filtration chromatography is a purification technique based on molecule size. Smaller particles enter agarose pores and are retained longer whereas bigger particles can flow through and elute earlier.

Gel filtration was used to purify the SLNs suspension from free, non-incorporated, Cy3 and CURC and from other possible impurities.

The stationary phase consisted of agarose gel, PBS was used as the mobile phase, eluent.

A volume of 250 μL of sample is loaded onto the column to be eluted by gravity; the eluent is added 1 mL at a time, waiting for the top of the column to dry before each subsequent addition. The fraction of interest containing SLNs is collected when the eluting drops appear opaque.

3.2.5.2.Dialysis

Dialysis is a purification technique based on molecule size and affinity for water. Small molecules, including salts, can pass the semipermeable membrane due to passive diffusion, depending on their size relative to the membrane pores.

Dialysis was also used to purify the SLNs suspension from free, non-incorporated, Cy3 and CURC and from other possible impurities.

Before preparing the dialysis a piece of dry membrane is boiled until it softens allowing its filling. 2 mL of SLNs suspension is loaded into the membrane which is then tightly closed and placed into a stirred flask filled with 1 liter of milliQ water.

Samples of 50 μL were collected hourly from inside the membrane to monitor compound release and purification quality.



Figure 3.1 – Dialysis setup

3.2.6. SLNs characterization

SLNs dispersed in water form a colloidal system, defined as a heterogeneous system of two immiscible phases, a continuous aqueous phase and a dispersed lipid phase with dimensions in the nanometers range.

Due to their high surface area, colloids are strongly influenced by interfacial phenomena.

While high surface tension promotes particle aggregation to reduce interfacial area and minimize interfacial energy, surfactants counteract this effect and provide stability.

Colloidal stability is also governed by kinetic and electrostatic factors.

Brownian motion, which depends on particle size, is the random movement of particles that induces diffusion counterbalancing sedimentation; this principle is exploited to determine particles hydrodynamic diameter by Dynamic Light Scattering (DLS) analysis by measuring fluctuations in scattered light.

Surface charge at the particle-water interface influences ions distribution around particles giving rise to an electrical double layer, the potential of which -measured as zeta potential- is a key indicator of colloidal stability.

3.2.6.1. Determination of mean diameter using DLS

DLS is used to determine the mean hydrodynamic diameter and the polydispersity index (PDI) of SLNs. PDI is a dimensionless measure of the width of particle size distribution, indicating the degree of uniformity of the sample: a low PDI (close to 0) reflects a monodisperse population with uniform particle sizes, whereas a high PDI (closer to 1) indicates a heterogeneous, polydisperse system.

A transparent cuvette containing the sample, prepared by diluting a few drops of SLNs suspension in MilliQ water, is placed in the instrument. A laser beam passes through the sample, and a detector measures the fluctuations in the intensity of scattered light. These fluctuations arise from the Brownian motion of particles in suspension; under the same temperature and viscosity conditions, smaller particles move more rapidly, producing faster changes in scattered light intensity.
Hydrodynamic radius (R_h) is calculated using Stokes-Einstein equation

$$R_h = \frac{BT}{6\pi\eta D} \quad (5)$$

where B is Boltzmann constant, T and η are temperature and viscosity of the system and D is the diffusion coefficient, obtained from the rate of intensity change of scattered light.
Measures are performed at 25°C with a 90° scattering angle.

3.2.6.2.Determination of Zeta potential

Zeta potential is a characteristic of particles that have a surface charge when dispersed in a liquid. As previously reported, the zeta potential value is correlated with the stability of a nanoparticulate suspension.

When particles are dispersed in a suspension, ions distribution around them changes, as counterions migrate closer to the particle surface, forming an electrical double layer. This layer consists of two regions: the inner region, known as Stern layer, tightly bound to the surface by strong electrostatic interactions and the outer, diffuse region characterized by weaker interactions.

The zeta potential is the electrical potential measured at the shear plane, which lies within the diffuse layer.

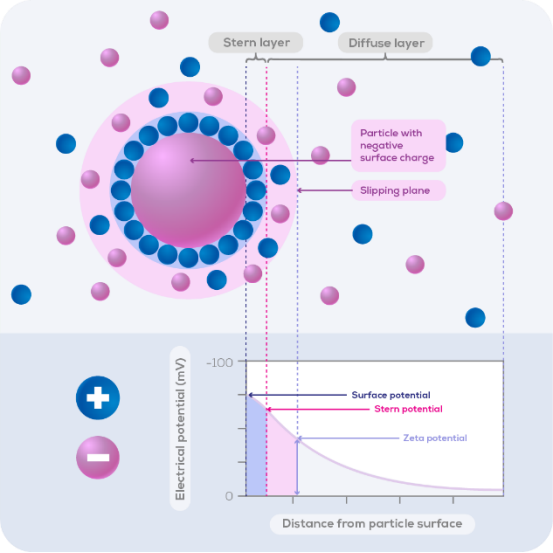


Figure 3.2 - schematic representation of zeta potential[35]

High absolute zeta potential, exceeding ± 25 mV, generates a strong electrostatic repulsion between particles, thus preventing aggregation and conferring enhanced colloidal stability to the suspension. In contrast, low zeta potential values indicate weaker repulsion and a higher tendency toward particle coalescence and precipitation.

The analysis is based on the principle that charged particles placed in an electric field migrate towards the pole with the opposite charge, indicating the sign of their surface charge, the velocity of this movement is used to calculate the zeta potential value.
For the measurement, SLNs suspension is diluted with MilliQ water and is placed in a specialized cuvette equipped with electrodes, inducing particle movement of the surface charged SLNs (electrophoretic mobility). A laser beam illuminates the sample, and the scattered light is detected; changes in the frequency of the scattered light are analyzed to determine the velocity of particle migration. From this mobility, the zeta potential is calculated, providing an indicator of the surface charge and stability of the colloidal system.

3.2.6.3. Observation by fluorescence microscopy

Fluorescence microscopy is a technique where the white light source is filtered by filters that allows only specific wavelengths to reach the sample, stimulating its fluorescence.

A fluorescent microscope is used to investigate the morphology of SLNs and the localization of the fluorescent dye Cy3 and of the drug CURC inside the SLNs. Fluorescence microscopy is also used to detect the presence of crystals or free (not-incorporated) Cy3 and CURC thereby allowing the efficiency of the purification procedures through background fluorescence assessment.
A green excitation filter is used to observe Cy3 fluorescence, which appears red. A blue excitation filter is used instead for CURC fluorescence, which appears yellowish.
Observations are made with a 50x objective.

3.2.6.4. Entrapment efficacy

Entrapment efficacy (EE%) of Cy3 and CURC within the SLNs is tested after purification by gel chromatography and dialysis.
Sample concentrations pre- and post-purification are obtained by high performance liquid chromatography (HPLC) analysis.
EE% is calculated as the ratio between the concentrations measured after purification and pre purification, multiplied by 100 to obtain the percentage.

3.2.7. SLNs fluorescence characterization

Fluorescence emission spectra are recorded at a scan speed of 10,000 nm/min with a data interval of 1 nm, excitation and emission bandwidth are set respectively to 1 nm and 5 nm.

Four samples are analyzed: blank SLNs, Cy3 SLNs, CURC SLNs and CURC-Cy3 SLNs.
Blank SLNs and CURC-containing SLNs are excited at 450 nm to detect the maximum CURC emission, while Cy3 SLNs are excited at 550 nm to obtain the maximum Cy3 emission. Emission spectra are collected respectively from 460 nm and 560 nm up to 750 nm.

Non-purified SLNs suspensions (pre-GF) are used as starting/reference material. Serial dilutions are prepared in MilliQ water ranging from 1:25 to 1:200 (corresponding to approximately 2.23 mg/mL to 0.28 mg/mL of SLNs suspension).
Spectra are processed using OriginPro software. Emission spectrum of blank SLNs is used as baseline reference and subtracted from all other spectra to remove background signal.

For each sample, maximum emission intensity is plotted against concentration to assess signal linearity and investigate the presence of possible quenching effects.

3.2.7.1. FRET test

Forster resonance energy transfer (FRET) is a physical phenomenon in which an excited donor molecule non-radiatively transfers some of its excited-state energy to a nearby acceptor molecule which then emits at its characteristic wavelength. The observable result is a decrease in donor fluorescent emission intensity and an increase in acceptor emission intensity. For FRET to occur, the two compounds forming the FRET couple must respect two conditions: they must be close in space, in the 1-10 nm range, and the donor emission spectrum and the acceptor excitation spectrum must significantly overlap. Because of these properties, FRET-based biosensors using fluorophore pairs, have been applied to study molecular interactions and dynamics inside cells.[36]

In order to investigate a possible FRET between co-encapsulated CURC and Cy3, FRET experiment is carried out. Spectra of both CURC-Cy3 SLNs and CURC SLNs are measured by using 450 nm as the excitation wavelength and maintaining apertures and emission wavelength unmodified.
The FRET Efficiency (%) is calculated using the following equation

$$E = \left(1 - \frac{F_{DA}}{F_D}\right) \cdot 100 \qquad (6)$$

where F_D is the fluorescence of the donor (CURC) in absence of the acceptor (Cy3) and F_{DA} is the fluorescence of the donor (CURC) in presence of the acceptor (Cy3).

As a control, a system where equal parts of Cy3 SLNs and CURC SLNs are mixed, is tested to assess whether the two dyes can give any FRET signal when in the same environment but non co-encapsulated.

3.2.8. HPLC-RP chromatographic analysis

High performance liquid chromatography (HPLC) is a qualitative and quantitative analytical technique used to identify and quantify components in complex mixtures.
Separation occurs due to different affinity and interaction of the analytes with the stationary phase and mobile phase: analytes with greater affinity for the stationary phase will elute later resulting in longer retention time inside the column.
In reverse phase (RP) chromatography the stationary phase is non-polar consisting of alkyl chain-functionalized silica, and the mobile phase is polar, generally water and organic solvents miscible with it.

Quantitative analyses of Cy3 and CURC are performed under identical conditions for column, eluents and flow rate although the two analytes are detected differently, the method is adapted from Takakura et al. [37]

- Stationary phase: Tracer Excel 120, RP C8, silica 5 μm, 250 mm x 4.6 mm.
- Mobile phase: 0.1% trifluoroacetic acid (TFA) in water (5%, v/v) and 0.1% TFA in acetonitrile (95%, v/v), isocratic elution
- Flow rate: 1 mL/min

3.2.8.1. HPLC analysis of Cy3

Cy3 is detected using a spectrofluorometric detector that excites the sample at a wavelength of 500 nm and detect emission at 603 nm, close to the maximum of fluorescence emission of the cyanine dye. Sample is not excited at the maximum of absorbance of 589 nm to avoid out-of-scale detection peaks. Fluorescence detection was preferred over UV-Vis detection due to its higher sensitivity at low analyte concentrations.
Under these conditions, retention time of Cy3 is 5.4 minutes.

Firstly, to quantify Cy3 in samples, a calibration curve must be constructed, starting from a stock solution which is prepared by solubilizing 1.56 mg of Cy3 powder in 2 mL of DMSO in a volumetric flask. Four serial dilutions of this stock solution are then prepared in methanol. The retention peak area (AUC) of each standard is plotted against its Cy3 concentration and the linear regression obtained by interpolating the points represents the calibration curve.

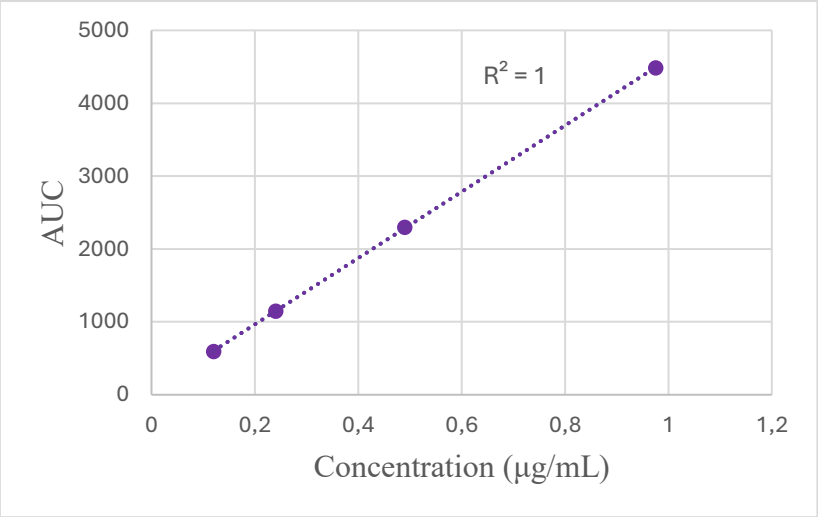


Figure 3.3 - Cy3 calibration curve

The equation of the calibration line obtained from the graph is:

$$y = 4{,}549.2x + 55.384 \quad (7)$$

this equation is used to calculate Cy3 concentration in the samples (x), by substituting the experimentally measured AUC value into y.

3.2.8.2. HPLC analysis of CURC

CURC is detected using a UV-Vis spectrophotometric detector at a wavelength of 425 nm, corresponding to the maximum of absorbance.
Retention time for CURC under these conditions is 3.2 minutes.

As in the previous paragraph, to quantify CURC in samples, calibration standards are prepared. A stock solution is prepared by solubilizing 1.3 mg of CURC powder in 10 mL of methanol in a volumetric flask. Serial dilutions of this stock solution are then prepared in methanol.
As for Cy3 calibration, AUC is plotted against CURC concentration to obtain the calibration curve.

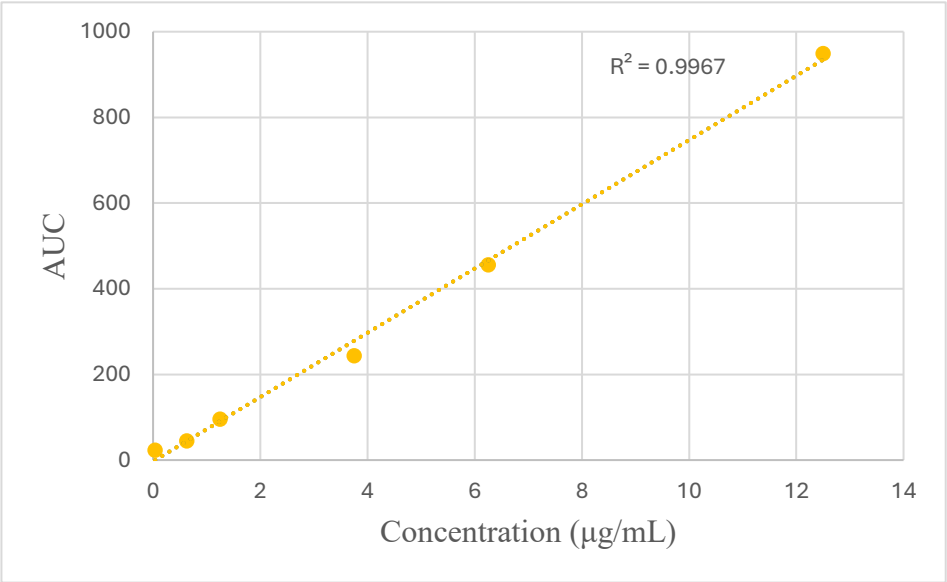


Figure 3.4 - CURC calibration curve

Equation of the calibration line extracted from linear regression of data is:

$$y = 75.013x - 3.022 \quad (8)$$

this equation is used to calculate CURC concentration in sample (x) by substituting the experimentally obtained AUC value into y.

3.2.9. In vitro release test

The release of Cy3 and CURC from Cy3-CURC SLNs is evaluated using a non-equilibrium dialysis method.

This approach allows the assessment of drug and dye release kinetics from SLNs under controlled conditions, providing insight into their potential bioavailability and stability.

In this approach, donor and receiver compartments are aligned and arranged circularly on two aligned rotating disks, allowing continuous stirring and efficient diffusion between compartments. A Durapore® polymeric membrane filter with 0.1 µm pores is inserted between the disks separating each donor compartment from its corresponding receiving compartment. The two disks are secured with screws and mounted on a shaft connected to a motor that provides rotation at 18rpm.

The donor wells are filled with 1.5 mL of sample to test, the receiver wells are filled with 1.5 mL of a 60% ethanol in water solution.

The analyzed sample are the following; solutions concentrations are chosen to be the same found inside the SLNs:

- Cy3 solution (10 μg/mL) in 60% ethanol in water
- CURC solution (625 μg/mL) in 60% ethanol in water
- Cy3-CURC SLNs before gel filtration (pre-GF)

At preset time points 1.5 mL are sampled from the acceptor wells and replaced with the same amount of fresh solution (60% ethanol in water). 1.5 mL aliquots are collected to avoid saturation of acceptor phases.
The concentration of Cy3 and CURC in each withdrawn sample are determined by HPLC analysis.

4. RESULTS AND DISCUSSION

The main aim of this work was to establish a reproducible, simple and cost-effective method to stably label solid-lipid nanoparticle (SLNs) with a fluorescent dye. These labeled SLNs were intended to gain insight into their intracellular fate.

At the best of our knowledge, fluorophores are generally encapsulated like drugs inside the SLNs core[9], unless covalently bound to the surface, a longer and costly step. Some studies have already developed such systems using customized dye, this is our aim as well to have a readily available labeling system that can be self-produced.

To study the behavior of the SLNs matrix in cells, it was necessary to develop SLNs in which the fluorophore (Cy3) is stably incorporated into the lipid matrix.

4.1. IODOCTYL-SUBSTITUTED BENZOINDOLE CYANINE DYE

4.1.1. Structure

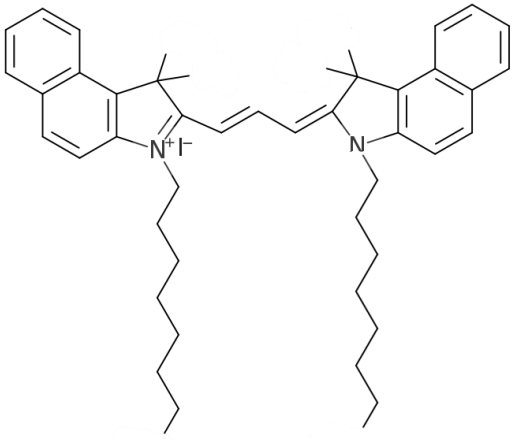


Figure 4.1 - Cyanine structure

Cyanine absorption and fluorescent properties arise from the presence of the fluorophoric moiety, represented by an electron-donating group and an electron-withdrawing group connected by a π-conjugated system.

Our cyanine dye has a base structure of two benzoindole groups linked by a trimethine bridge. To ensure better fluorescence properties, the nitrogen of both indole rings is quaternized by substitution with alkyl groups.

An iodo-octane chain has been selected as a substituent to confer a strong lipophilic character to the cyanine, the resulting dye is expected to exhibit low solubility and reduced fluorescence

emission in aqueous solutions but bright fluorescence in lipid phases.[38] The long alkyl chains were expected to intercalate into the lipid core of SLNs, with the aim of incorporating the cyanine dye as part of the SLN structure rather than encapsulating it as a drug inside the nanoparticles.

Each indole ring is fused to a benzene ring, forming the benzo[e]indole group, this modification causes a red-shift of the usual abs/em spectra of trimethine cyanine dyes and helps increasing structure rigidity and thermostability[39]. The extended conjugated system enhances electron delocalization stabilizing the structure. This results in a smaller gap between the higher occupied molecular orbital and the lower unoccupied molecular orbital (HOMO-LUMO gap) meaning that less energy is required to excite the molecule thus inducing a bathochromic shift in absorption.[40]
The resulting fluorescence emission of the cyanine dye is bright pink.

4.1.2. Synthesis

Cyanine dye synthesis is carried out in two main steps.
Firstly, compound AI1 is obtained by quaternization of benzo[e]indole nitrogen with an iodo octane chain. Subsequently, the corresponding cyanine dye is synthetized via a double condensation reaction that couples two benzo[e]indole units through a methine bridge.

The N-alkylation step converts the nitrogen atom to a cationic quaternary ammonium center, enabling the delocalization of the positive charge over the indole ring. This delocalization is essential for the fluorescence properties of cyanine dye.
The methyl group in position 2 already shows great reactivity due to the positive charge on the quaternary ammonium, deprotonation of methyl group by pyridine further enhances its nucleophilicity, this allows a nucleophilic attack to the imine carbon of the methine bridge.
Acetic anhydride acetylates the ammine of the methine bridge forming an amide, that is both a good leaving group and enhances the electrophilicity of the adjacent imine carbon.
Finally, the second benzo[e]indole group performs a nucleophilic attack on this carbon forming the complete cyanine dye. [41]

4.1.3. Spectrophotometric properties

Absorption spectrum of AI2 sample in methanol is reported in figure 4.2.

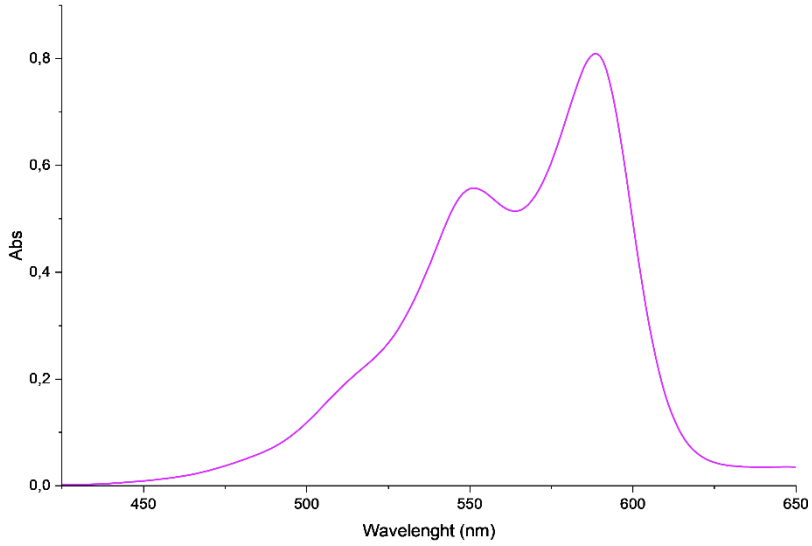


Figure 4.2 - AI2 absorption spectrum

The main absorption peak is observed at 589 nm, in the green-yellow region of the visible spectrum.

The main peak corresponds to the electronic transition from the ground state to the first excited state ($S_0 \rightarrow S_1$), it is attributed to $\pi \rightarrow \pi^*$ transitions along the methine bridge.
The fine structure of spectrum, visible as peaks and shoulders at wavelengths shorter than the main absorption band, arises from vibronic transitions, thereby the possibility of observing transitions from ground state to higher vibrational levels of excited state (e.g. $S_0(v=0) \rightarrow S_1(v=1)$).
In AI2 this shoulder peak shows lower absorption intensity because, according to Franck-Condon principle, in symmetric cyanine dye the vibrational overlap is maximal for $0 \rightarrow 0$ vibronic transitions. This is explained by the fact that their equilibrium geometries of ground and excited state are very similar.[42][43]

The main peak at 589 nm shows a bathochromic shift to longer wavelengths compared to other commercially available Cy3 dyes that have absorption peaks around 550 nm (e.g. Cy3-NHS ester [44]), this is imputable to the addition of the benzene ring to the indole that increases the

size of the conjugated system. The alkyl chain, instead, has no measurable effect on absorption wavelength.[23]

From absorption spectra recorded at increasing concentrations (figure 4.3, refer to section 3.2.3.1.) the absorbance values at the maximum absorption wavelength are obtained.
The absorbance values are plotted as a function of concentration to determine the molar absorption coefficient as the slope of the regression (Figure 4.4).

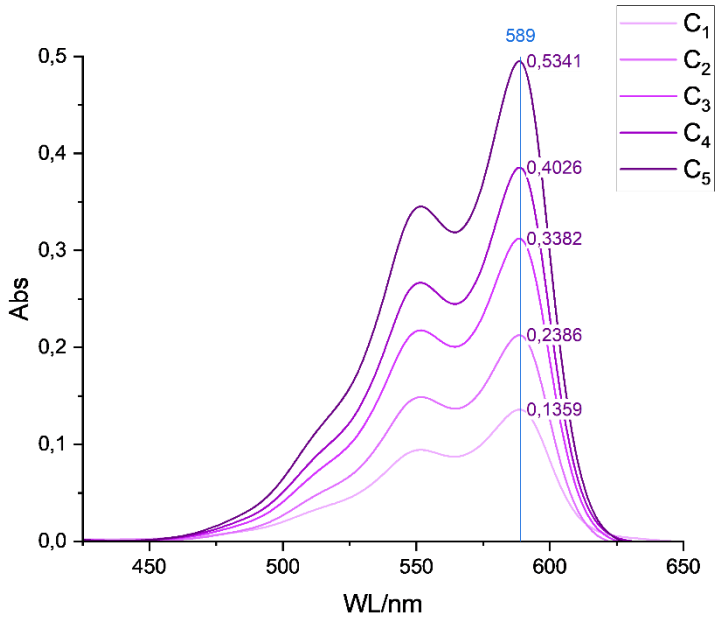


Figure 4.3 - Absorption spectra of AI2

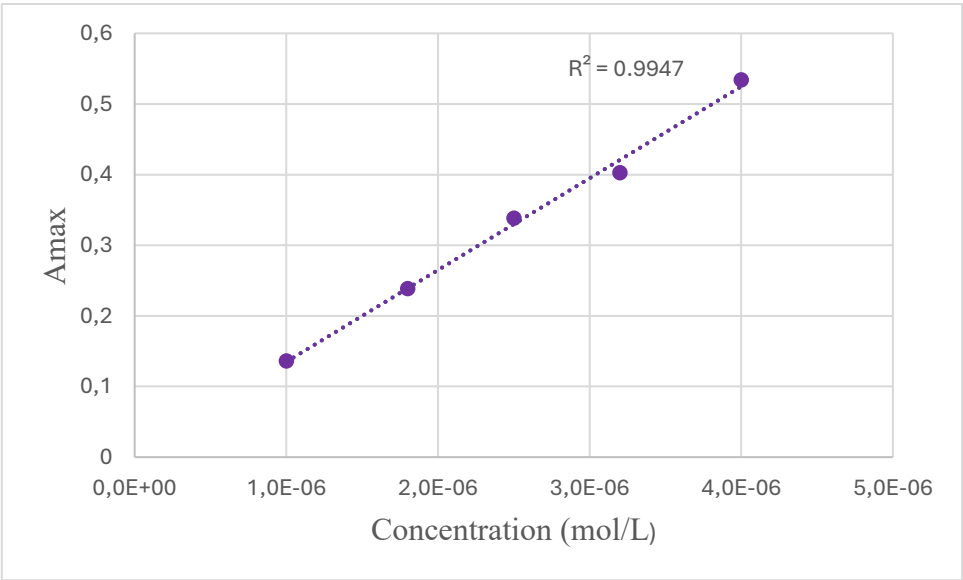


Figure 4.4 - Calibration curve of AI2

The equation of the linear regression is the following

$$y = 129{,}945x + 0.005 \quad (9)$$

indicating 129,945 $Lmol^{-1}cm^{-1}$ as the value of the molar absorption coefficient (ε).

ε is a measure of a compound ability to absorb light at its maximum absorption wavelength, AI2 shows a value within the typical range of other cyanine dyes, indicating good absorption efficiency.

4.1.4. Spectrofluorimetric properties

Emission spectra of AI 2 are recorded from dilutions in methanol, of a stock solution in DMSO, at increasing concentration; dilutions are maintained in the range of 10^{-6} M, to ensure absorbance values under 0.2-0.3 a.u.

Excitation at 550 nm, corresponding to the shoulder peak, is chosen to allow for an efficient excitation and for the acquisition of the complete emission spectrum, as a small Stokes shift is expected.

The peak of emission is observed at 604 nm, with a Stokes shift of 15 nm. In the most concentrated sample, the peak is slightly shifted at 606 nm, the small 2 nm red shift may be attributed to inner filter effect that at higher concentrations causes partial reabsorption of emitted light.

Alkyl chain substitution has no effect on emission wavelength.

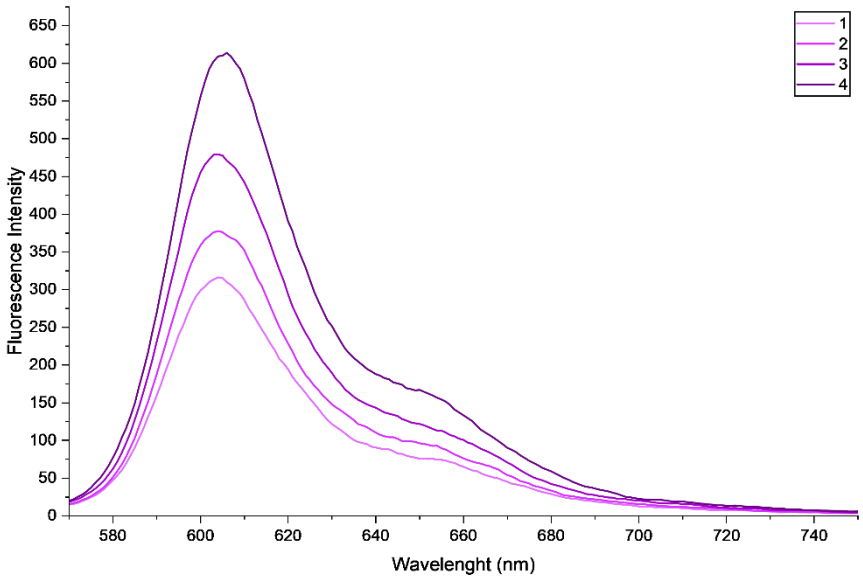


Figure 4.5 - Emission spectra of AI 2

Quantum yield (Φ) which describes the efficiency of fluorescence emission is, together with ε, a defining parameter to characterize a fluorophore. Sometimes these two parameters are combined in a single metric called Brightness that is obtained by multiplying their values, it accounts for both the efficiency in absorbing light and in emitting it. Cyanines are known to have good brightness values even with lower quantum yield thanks to the high ε that makes them strong absorbers.[27]

By plotting absorbance at excitation wavelength (Abs) vs integrated area of fluorescence emission spectra (F) the quantum yield is obtained (refer to 3.2.3.2.).

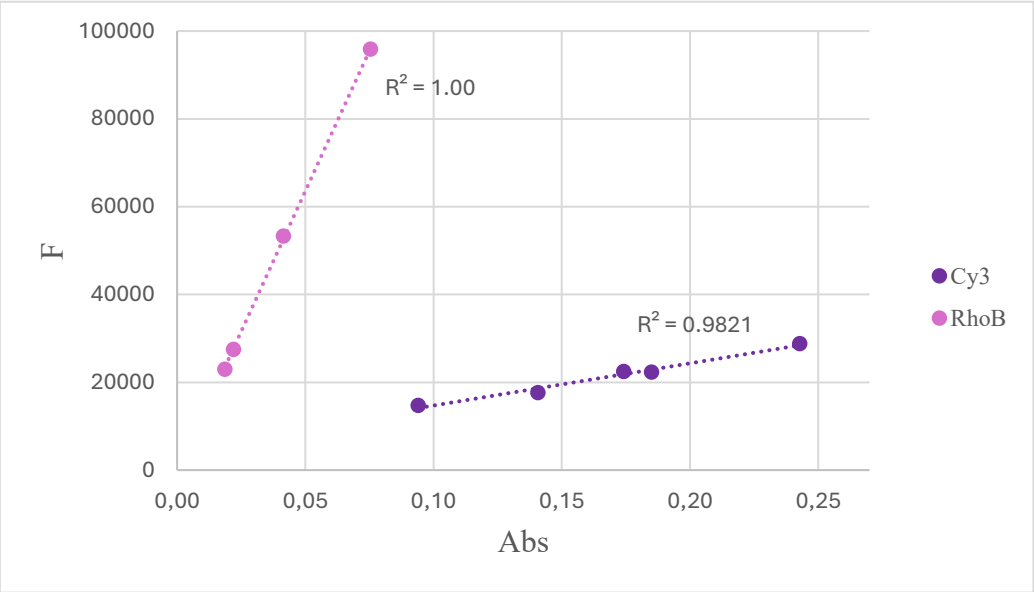


Figure 4.6 - Abs vs F plot of Cy3 and RhoB

The equations of the regressions obtained from the graph are respectively

$$y = 1{,}277{,}999.79x - 349.15 \quad \text{(RhoB)} \tag{10}$$

$$y = 96{,}138x + 5{,}095.6 \quad \text{(Cy3)} \tag{11}$$

The slope of the regressions is an indicator for fluorescence efficiency of Cy3 sample and of RhoB reference standard, the steep slope of RhoB indicates a very high fluorescence efficiency whereas Cy3 has a much lower efficiency.

The quantum yield calculated for Cy3 is 5.26%.

This value is relatively low for a fluorescent dye, however a low quantum yield is not uncommon for cyanine dyes. Furthermore, our cyanine dye will be incorporated into nanoparticles the resulting quantum yield is expected to increase: encapsulation of dyes into a

solid matrix is, in fact, known to enhance fluorescence efficacy. This effect is partly due to the high local concentration of dye molecules within each nanoparticle (NP) and partly related to the encapsulation itself, the NP rigid matrix can restrict molecular vibrations and rotations, thus reducing non-radiative decays that compete with fluorescence emission.[45]

4.2. PREPARATION AND CHARACTERIZATION OF SLN

Initial attempts to formulate Cy3 SLNs involved direct addition of 0.3 mg of Cy3 powder to the formulation after solubilizing Epikuron®200. However, Cy3 did not completely solubilize and the resulting µE could not be obtained. The SLNs obtained under these conditions exhibited excessive background fluorescence and irregular morphology, leading to the formulation being discarded.

Subsequent formulations were prepared using different volumes of the Cy3 in S-EtOAc stock solution. The formulation containing 100 µL of stock solution is discarded because the µE is not obtained and because the final color of the suspension and its fluorescence was too bright. The formulations containing 10 and 25 µL of stock solution were also discarded since their color is too faint as can be appreciated in Figure 4.7 (B). Indeed, given that the SLNs suspension must be diluted 1:100 prior to administration, these formulations were expected to yield insufficient fluorescence intensity.

The formulation containing 50 µL of Cy3 stock solution demonstrated an appropriate balance between fluorescence intensity and visual appearance and successfully formed a µE as seen in Figure 4.7 (A). The concentration of Cy3 added, considering a final volume of the suspension of 4 mL, is 10 µg/mL Therefore, this composition was selected for further studies.

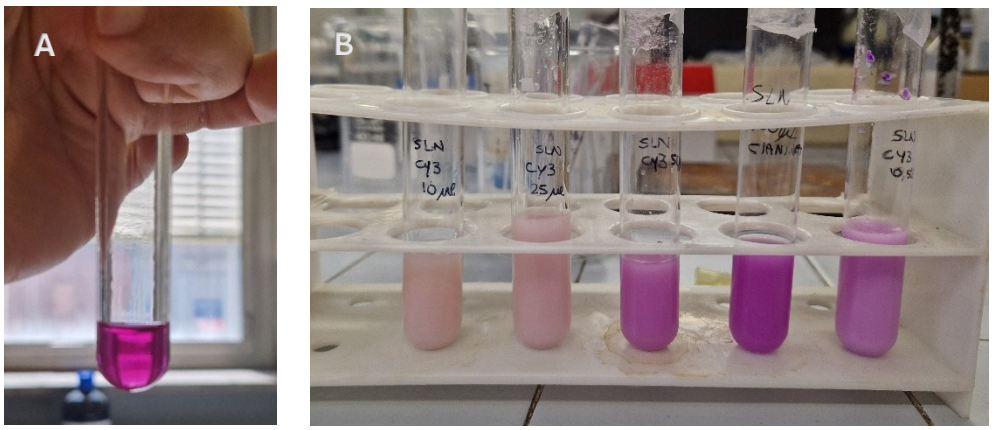


Figure 4.7 - (A) Cy3 µE , (B) Cy3 SLNs suspension from left to right containing 10, 25, 50, 100 µL of stock solution and 0.3 mg of cyanine powder.

The CURC-Cy3 SLNs formulation containing 50 µL of Cy3 in S-EtOAc stock solution (39 µg) and 2.5 mg of CURC is selected over the formulation with 5 mg of CURC based on the visual appearance of the final SLNs suspension (Figure 4.8 (A) and (B)) and its background fluorescence intensity.

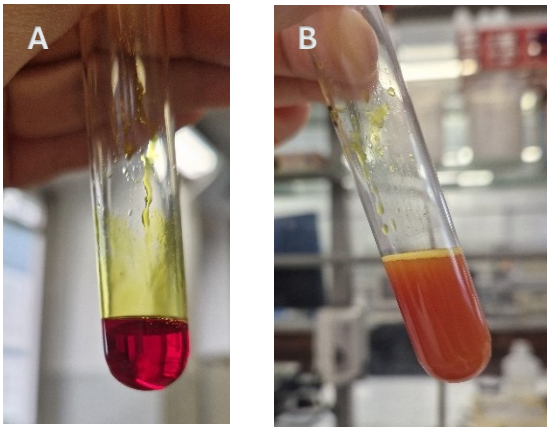


Figure 4.8 - (A) CURC-Cy3 µE, (B) CURC-Cy3 SLNs suspension.

The initial confirmation of SLNs formation is performed by DLS which verify the presence of nanometric structures.

Encapsulation of Cy3 and CURC is further assessed by fluorescence microscopy. Using different filters to detect each compound (Cy3 and CURC), SLNs appeared as bright fluorescent spots; when the same SLN is visible under both filters, this indicates the co-encapsulation of Cy3 and CURC within the same nanoparticle, as indicated by Figure 4.9.

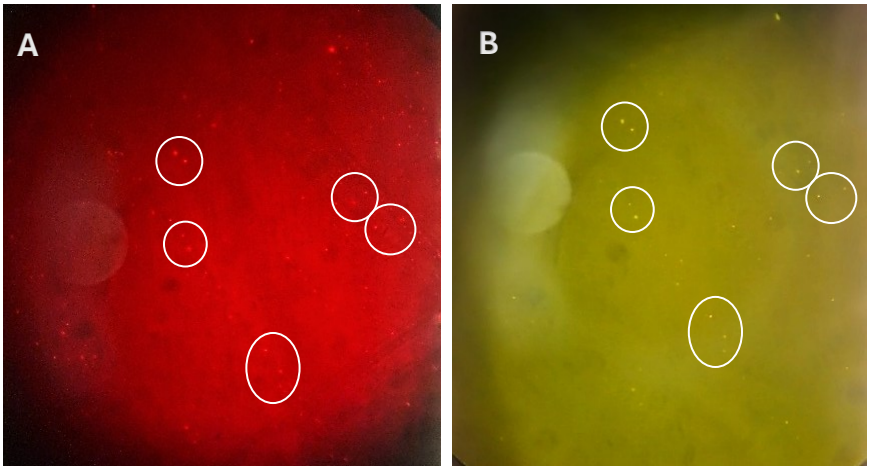


Figure 4.9 - Images of fluorescence microscopy. Circled, some of the SLNs visible in both conditions, indicating co-encapsulation of both drugs. (A) Green filter excitation to detect red Cy3 emission. (B) Blue filter excitation to detect yellow CURC emission.

Field Emission Scanning Electron Microscopy (FESEM) is an electronic microscopy technique that we used to obtain clear 3D images of nanoparticles.

Due to technical issue in the preparation of the samples, FESEM imaging was not optimal, as the samples resulted contaminated by non-structured organic matter maybe as a results of the use of contaminated water for the dilution of the SLNs during the preparation of the sample. Nevertheless, in the FESEM images reported in Figure 4.10, some roundish particles (ca. 100 nm) of CURC-Cy3 SLNs (Figure 4.10 (A)) and of Cy3 SLNs (Figure 4.10 (B)).

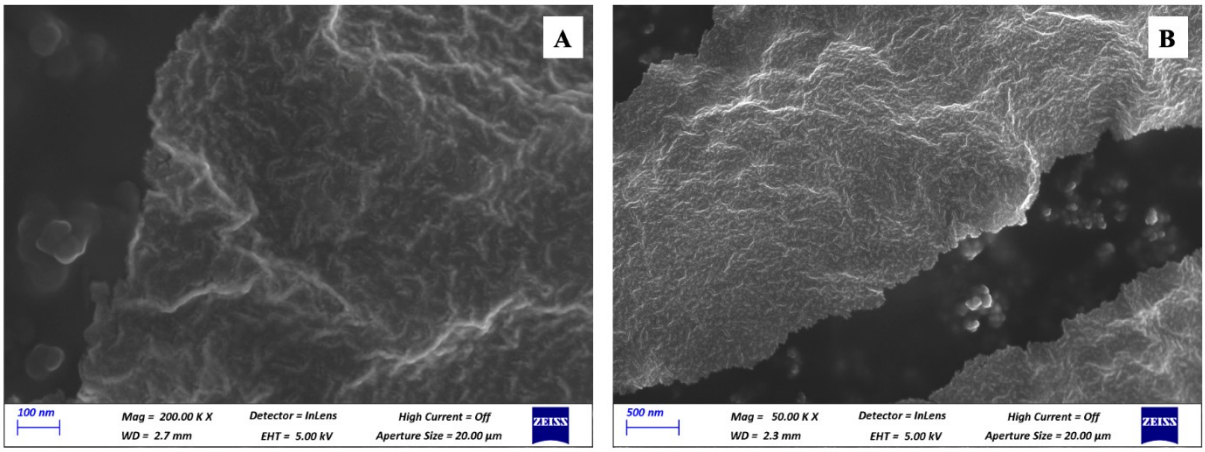


Figure 4.10 – FESEM images of (A) CURC-Cy3 SLNs and (B) Cy3 SLNs.

4.2.1. Determination of mean diameter using Dynamic Light Scattering (DLS)

DLS analyses are carried out as described in Section 3.2.6.1. The mean diameters and polydispersity indexes (PDI) of Cy3 SLNs and CURC-Cy3 SLNs, measured before purification (pre), after gel filtration (post GF) and one hour post-dialysis are reported in Table 4.1 Mean diameter of blank SLN pre is also reported.

Table 4.1 - DLS results

Sample	Diameter (nm)	PDI
Blank SLN pre	272.2 ± 2.0	0.208
Cy3 SLN pre	313.6 ± 8.4	0.279
Cy3 SLN post GF	295.3 ± 4.6	0.262
Cy3 SLN post dialysis	299.1 ± 6.8	0.288
CURC-Cy3 SLN pre	306.4 ± 5.9	0.230
CURC-Cy3 SLN post GF	291.1 ± 1.5	0.261
CURC-Cy3 SLN post dialysis	336.4 ± 8.4	0.294

SLNs diameters are generally consistent across all analyzed formulations, with values around 300 nm. Diameters of SLNs containing CURC or Cy3 in the core structure are slightly larger compared to blank SLNs, but the overall size increase is minimal.

Although these mean diameters are slightly above the recommended threshold for intravenous administration (< 200 nm), which favors enhanced permeability and retention (EPR) effect and reduces clearance by the reticuloendothelial system (RES)[46], these nanoparticles are however suitable for in vitro cell studies. Cells can internalize nanoparticles through various mechanisms allowing preliminary studies on SLNs localization within cells after internalization.[47]

PDI values are in the 0.2-0.3 range indicating satisfactory sample homogeneity, minor variations may be attributed to SLNs aggregation or to the presence of not-incorporated drug aggregates.

4.2.2. Determination of zeta potential

Zeta potential analyses are carried out as described in Section 3.2.6.2. The zeta potential of Cy3 SLNs and CURC-Cy3 SLNs were measured before purification (pre), after gel filtration (post GF) and one hour post-dialysis as reported in Table 4.2.

Table 4.2 - Zeta potential results

Sample	Zeta potential (mV)
Blank SLN pre	-21.8 ± 1.4
Cy3 SLN pre	-24.4 ± 1.1
Cy3 SLN post GF	-30.6 ± 2.4
Cy3 SLN post dialysis	-23.3 ± 0.4
CURC-Cy3 SLN pre	-23.7 ± 1.8
CURC-Cy3 SLN post GF	-20.2 ± 0.6
CURC-Cy3 SLN post dialysis	-19.6 ± 0.6

All SLN formulations exhibited a negative surface charge, attributable to the presence of Epikuron®200, a negatively charged phospholipid. The measured zeta potential values, with absolute magnitudes of approximately 20 mV, suggest moderate colloidal stability driven by electrostatic repulsion between nanoparticles. This charge values suggest reduced immediate aggregation; this may not be sufficient to ensure long-term stability of the suspensions, and partial aggregation over time cannot be excluded. Cyanine, being a cationic dye inserted onto the nanoparticle surface, influence the absolute value of zeta potential.

These results, taken together with those from DLS analyses, indicate a good colloidal profile of SLNs and sufficient stability to perform initial *in-vitro* studies. This conclusion is supported by their nanometric size (around 300 nm), narrow size distribution and zeta potential values which are indicative of a stable suspension.
Moreover, values show limited variations across purification steps by gel filtration and dialysis, suggesting that both strategies are suitable for purifying SLNs from impurities without substantially altering their physicochemical characteristics.

4.3. ENTRAPMENT EFFICIENCY EVALUATION

4.3.1. Quantification by HPLC

The two previously described purification methods were used to determine the entrapment efficacy (or loading efficiency) of Cy3 and CURC within the SLNs.

Quantifications are obtained by HPLC analysis, using Eq.7 and Eq.8 to calculate sample concentrations.

An initial analysis is performed on SLNs immediately after synthesis, before any purification. For SLNs, 10 µg/mL of Cy3 dye are added during formulation. HPLC analyses of SLNs prior to purification show Cy3 concentrations ranging from 8.2 to 9.7 µg/mL indicating only minimal dye loss during the synthesis process, likely attributable to human or instrumental errors.

In CURC-Cy3 SLNs, 625 µg/mL of CURC powder are added during formulation. HPLC analyses of these SLNs prior to purification show CURC concentrations ranging from 565 to 602 µg/mL indicating a higher absolute loss of material compared to Cy3. This is likely because CURC is added in powder form, which can stick to the vial walls and prevent its complete incorporation into the SLNs during synthesis.

Gel filtration (GF), a form of size exclusion chromatography, and dialysis are then used to purify the samples from non encapsulated molecules. Dialysis was initially tested for six hours; however it was observed that the concentration of the entrapped compound did not decrease significantly after one hour. Therefore, a one-hour dialysis was adopted for the following analyses.

EE% is calculated as described in section 3.2.6.4. Results are summarized in Table 4.3.

Table 4.3 - Entrapment efficacy of Cy3 and CURC

Sample	Cy3 EE%	CURC EE%
Cy3 SLN post dialysis	64.4 ± 1.6	
Cy3 SLN post GF	84.2 ± 3.9	
CURC-Cy3 SLN post dialysis	81.2 ± 4.0	77.9 ± 3.9
CURC-Cy3 SLN post GF	89.5 ± 2.2	83.8 ± 3.7

Both Cy3 and CURC show higher EE% after GF compared to dialysis, with statistical significance.

This behavior after dialysis may be attributed to the longer exposure (one hour vs few minutes in GF) to the aqueous environment, which can facilitate partial diffusion and release of the molecules out of the nanoparticle matrix.
Overall, the results confirm that both compounds can be efficiently encapsulated in SLNs, with gel filtration providing an optimal purification method.

Performing multiple analyses, small and generally not significant variations (± 5%) in loading efficiency are found between different sample.
In GF purification is observed that SLNs and free-Cy3 co-elute causing a possible overestimation of EE% due to the not complete purification from non encapsulated dye. In contrast, EE% values of CURC after GF purification are more stable across analyses since free CURC is observed to elute in a completely different fraction than SLNs.
For this reason, GF is chosen as the purification method for subsequent in vitro drug release studies.

4.3.2. Observation by fluorescence microscopy

A further qualitative analysis of SLNs is performed by fluorescence microscopy.
Samples observed before purification exhibit high background fluorescence, covering most signals from SLNs.
Dialyzed samples showed lower background fluorescence but many SLNs appeared aggregates and elongated, not spherical, deeming the purification technique not optimal.
Gel-filtrated samples showed low background fluorescence as well but also predominantly spherical SLNs. Together with better loading efficiency results, this supports the choice of GF as the main purification technique.

4.4. SLN FLUORESCENCE CHARACTERIZATION

Serial dilutions of SLN suspension were prepared in milliQ water at decreasing concentrations, as described in section 3.2.7., and their fluorescence emission spectra are recorded.
The spectra are presented graphically in Figure 4.11, with darker shades corresponding to higher concentrations and lighter shades to lower concentrations.
The concentration of the SLNs suspensions is estimated as the sum of all lipid components used in the formulation (TL, Epikuron®200, CURC) divided by the final volume. Therefore, the

resulting concentrations are and 56 mg/mL for blank SLNs and Cy3 SLNs and 56.77 mg/mL for CURC SLNs and CURC-Cy3 SLNs. The maximum fluorescence emission values are plotted against sample concentration to assess whether emission intensity increased linearly with concentration.

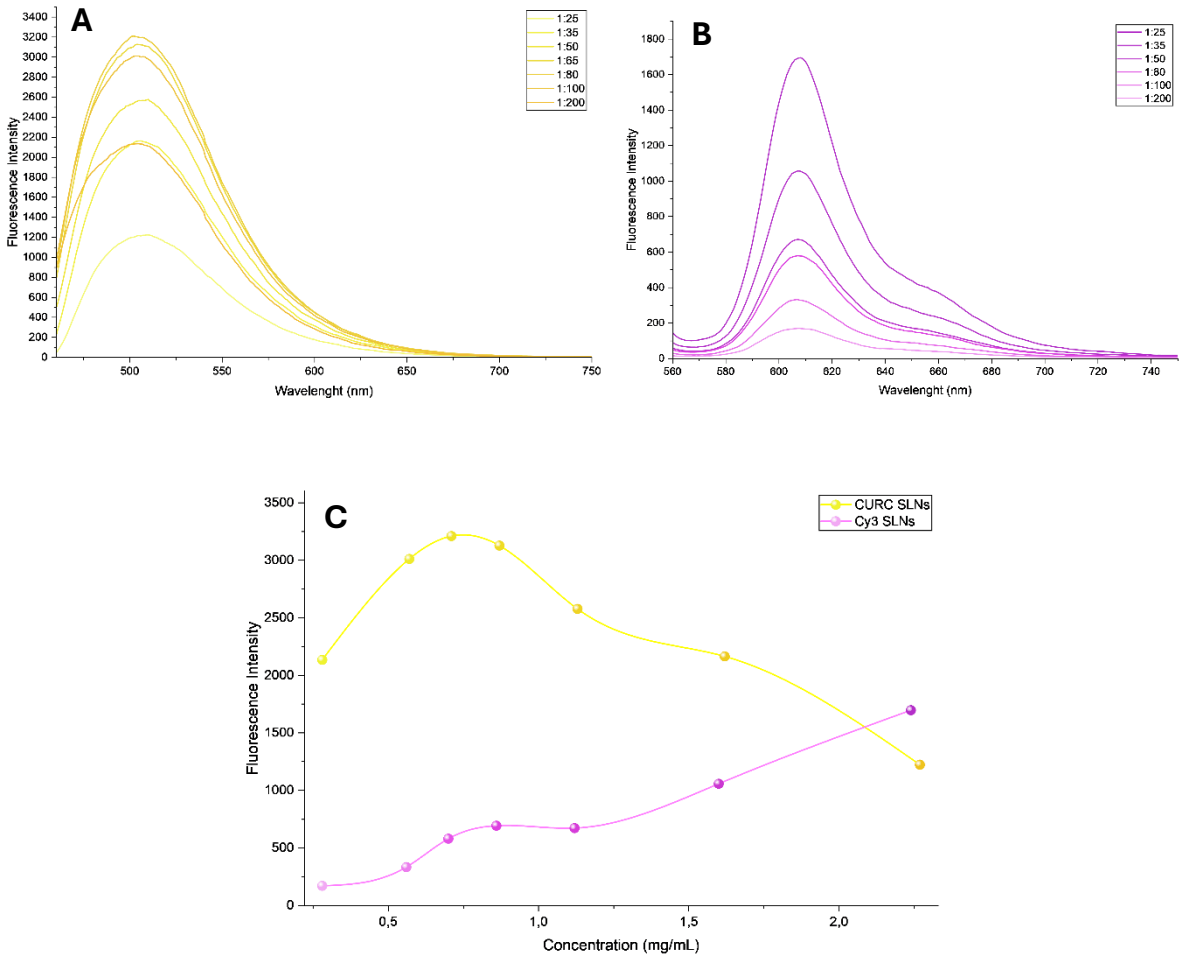


Figure 4.11 – (A) CURC SLNs emission spectra excited at 450 nm. (B) Cy3 SLNs emission spectra excited at 550 nm. (C) CURC and Cy3 fluorescence intensity over concentration.

CURC SLN emission spectra (Figure 4.11 (A)) appear broadened, with almost 100 nm of width at half maximum fluorescence. This is consistent with CURC emission in solution[48] and with the relatively high concentration of CURC in the SLNs core. The spectra are broader compared to other commonly used fluorophores, including Cy3, which can be attributed to the lower rigidity of CURC that, allowing vibrational relaxation, leads to less efficient and broader fluorescence emission.

Cy3 SLN emission spectra (Figure 4.11 (B)) closely resemble those of Cy3 in solution (Figure 4.5); no broadening of the main peak is observed and the shoulder-to-peak ratio remains similar.

As previously observed for Cy3 in solution, the emission peak slightly red-shifts as the dye concentration increases. These observations indicates that Cy3 is uniformly distributed within the SLNs, without forming aggregates.
These results show that the incorporation of Cy3 inside SLNs preserves their optical characteristics, making them suitable for application in optical imaging.

Despite small variations due to slight heterogeneity of the starting material, the intensity of Cy3 SLN emission shows an almost linear increase in fluorescence emission with increasing concentration.
The intensity of CURC emission in CURC SLNs, instead, displays a linear increase up to approximately 0.7 mg/mL, after which the signal decreases. This behavior indicates that, at high SLN, and therefore CURC, concentration, fluorescence quenching occurs, likely due to self-absorption effects in SLN matrix.

Based on previous studies in our laboratory, SLNs are typically administered to cells for *in vitro* studies at dilution of 1:100 or higher (corresponding to ca. 0.6 mg/mL). The fact that the emission intensity remains linear within this dilutions range is favorable to ensure reliable fluorescence measurements.

4.4.1. FRET analysis

CURC is excited at 450 nm and shows a peak emission at around 510 nm, with its emission tail extending to approximately 625 nm. Cy3 has a maximum absorption at 589 nm but is generally excited at 550 nm, corresponding to its shoulder peak. These observations indicate that the emission spectrum of CURC and the excitation spectrum of Cy3 overlap optimally as seen in Figure 4.12, making them an efficient FRET pair.

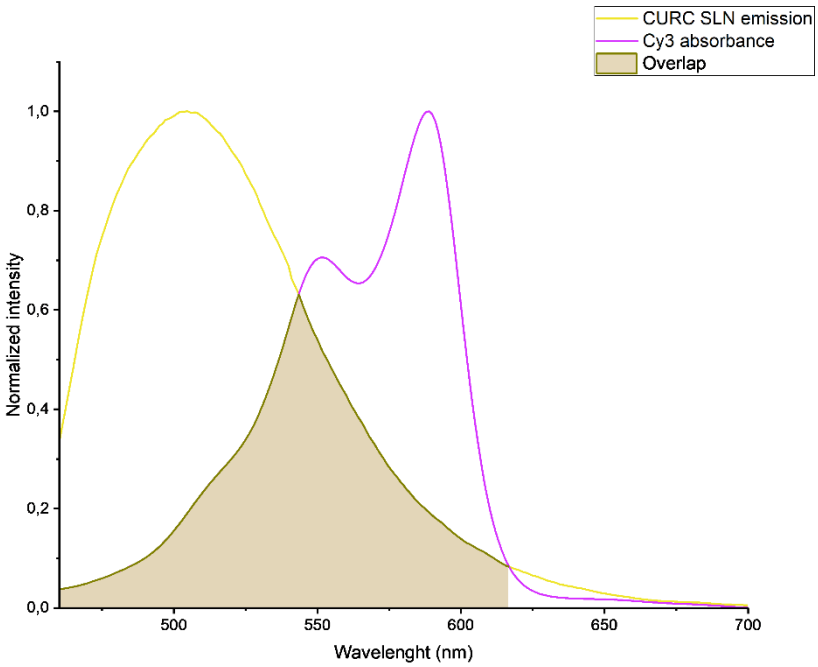


Figure 4.12 – CURC SLNs emission spectrum excited at 450 nm, Cy3 absorbance spectrum. The overlapping area where FRET phenomenon can happen is highlighted in brown.

CURC-Cy3 SLNs spectra are recorded with excitation at 450 nm to evaluate FRET.

Spectra of CURC SLNs and Cy3 SLNs at the same dilutions and under identical conditions are also collected as controls, allowing quantification of energy transfer and confirming the expected decrease in CURC emission and the corresponding increase in Cy3 emission.

Another control is performed by mixing equal parts of CURC SLNs and Cy3 SLNs in a vial and analyzing it at the same dilutions as the samples. Since CURC and Cy3 are encapsulated in different SLNs, they are not within the 10 nm range and FRET is not expected. This is experimentally confirmed, as the emission spectrum of this sample, excited at 450 nm, closely resembles that of CURC SLNs, with no significant Cy3 signal.

CURC-Cy3 SLNs spectra, recorded at various dilutions, are plotted in Figure 4.13 (A-B-C) as previously described for CURC SLNs and Cy3 SLNs. The fluorescence intensity-concentration curve (Figure 4.13 (D)) shows a very similar trend to that of CURC alone, fluorescence intensity reaches a maximum around 0.8 mg/mL and then decreases, consisting with CURC quenching at higher concentrations.

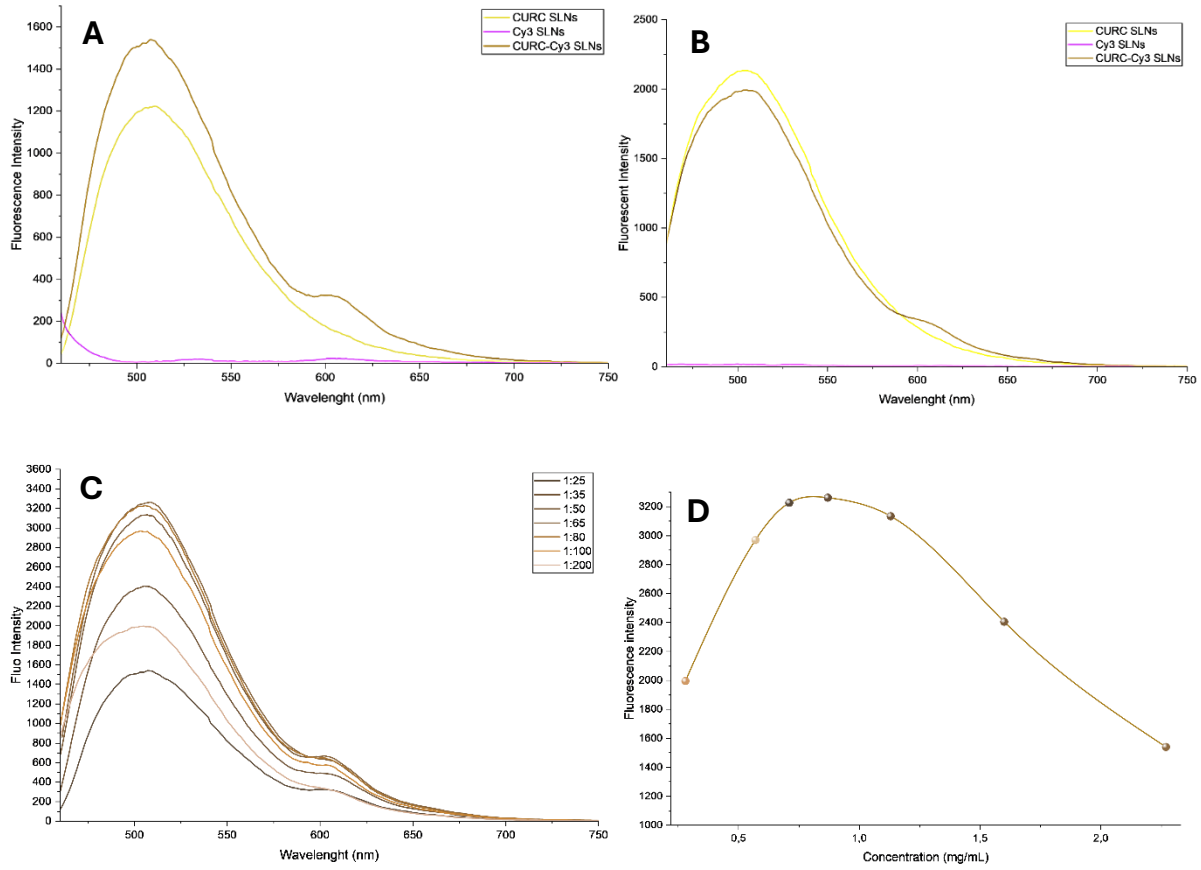


Figure 4.13 - CURC SLNs, Cy3 SLNs, CURC-Cy3 SLNs emission spectra excited at 450 nm. (A) 1:25 SLNs dilution. (B) 1:200 SLNs dilution. (C) CURC-Cy3 SLNs emission spectra excited at 450 nm. (D) CURC-Cy3 SLNs fluorescence intensity over concentration.

Figure 4.13 (B) is used to calculate FRET based on decrease of donor emission, according to Eq. 6, obtaining a value of 6.45%.

The measured FRET efficiency is likely underestimated because the donor (CURC) is present in large excess compared to the acceptor (Cy3). As a result, the strong emission from CURC molecules that do not transfer energy to Cy3 dominates the overall emission signal.

Another way to estimate FRET efficiency is by focusing on acceptor emission. To do so, the emission of Cy3 obtained by FRET in CURC-Cy3 SLNs has been isolated by curve fitting (red curve in Figure 4.14) and compared to Cy3 emission obtained by exciting at 450 nm Cy3 SLNs (pink curve) and to CURC-Cy3 SLNs emission excited at 550 nm (violet curve). The latter represents the maximum Cy3 emission in CURC-Cy3 SLNs as it is obtained by exciting the sample at the optimal wavelength for Cy3 emission.

Considering that emission of Cy3 for direct excitation at 450 nm is negligible (37 a.u. of emission intensity), we can observe that exciting CURC-Cy3 SLNs at 450 nm yields an emission intensity which is ca. 13.5% of that obtained by exciting Cy3 at its maximum (231 vs. 1750 a.u. of emission intensity).

With this respect, the estimated FRET efficiency increases to ca. 13.5%.

Considering that the large excess of donor does not meet the optimal requirement for FRET, this should be considered a very good result.

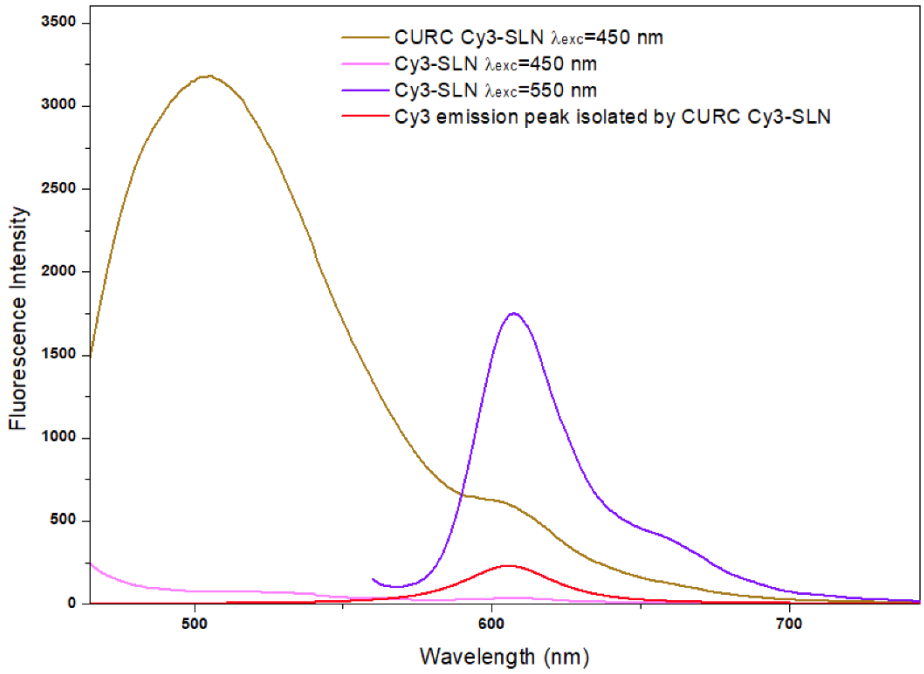


Figure 4.14 – Comparison between CURC-Cy3 SLNs emission obtained through excitation at 450 nm and emission of Cy3 SLNs excited at 450 nm and 550 nm. Cy3 emission profile isolated by curve fitting from spectrum of CURC-Cy3 SLNs excited at 450 nm, representing Cy3 emission generated by FRET, is also represented.

4.5. IN VITRO RELEASE TEST

In vitro release experiments are carried out to evaluate the release of CURC and Cy3 from SLNs in comparison with their corresponding free solution. The tests are performed using a dialysis rotating device and monitored over a period of 24 hours.

Quantification of released dye and drug is achieved through HPLC analyses.

Release profiles, expressed as the percentage of compound released over time, have been obtained for the following samples: free CURC and free Cy3 solutions as well as CURC-Cy3 SLNs.

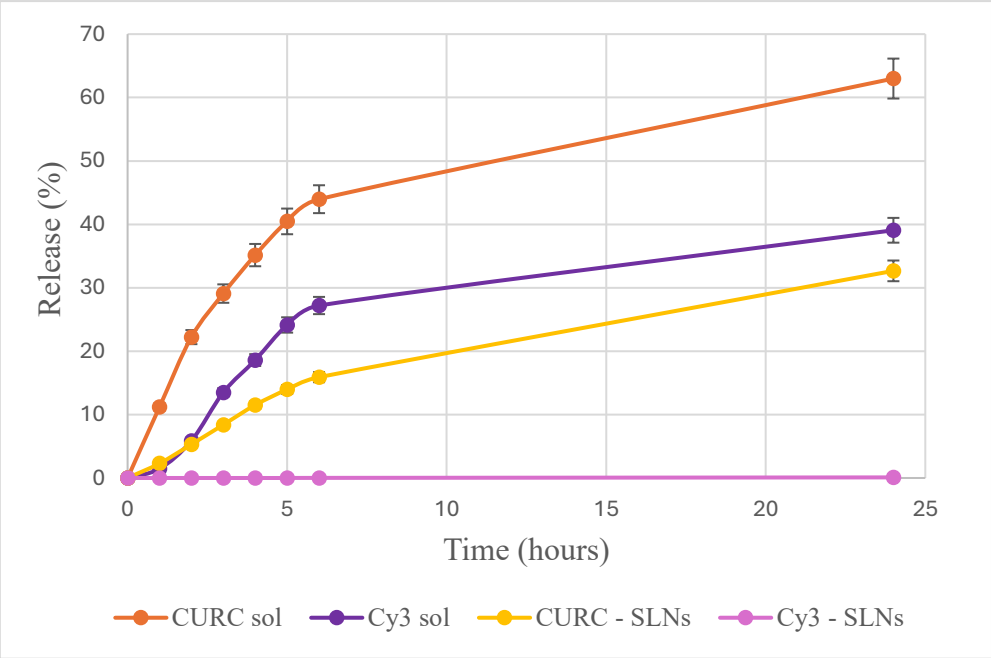


Figure 4.9 – CURC and Cy3 release profiles

A clear difference can be observed between the release profiles of CURC and Cy3 from SLNs compared to those of the corresponding free solutions used as references.

Both free CURC and free Cy3 solutions show a marked initial burst release (dose dumping) followed by a steady release phase. In contrast SLNs display an evident slower release, indicating that CURC and Cy3 have been successfully encapsulated within the nanoparticles. This also suggests that SLNs remain structurally intact during the experiment without undergoing rapid disassembly, allowing a continuous and controlled release of the compounds.

When comparing the free solutions, CURC shows a faster release than Cy3 reaching approximately 63% vs. 40% permeation over 24 hours, respectively.

This difference can be attributed to three main factors. First, the distinct physicochemical properties of the two molecules strongly influence their diffusion across the membrane.
Second, the donor-phase concentrations are markedly different (625 µg/mL for CURC vs. 10 µg/mL for Cy3), which may as well affect diffusion. Nevertheless, this gap of concentration is necessary to have consistency with the relative amounts of the two molecules entrapped in SLNs, as previously reported. While CURC needs to be tested at higher concentration to ensure therapeutic efficacy, as proven in previous works; Cy3 thanks to its strong signal-to-response ratio can be used as a fluorescent probe at much lower concentration.
Third, direct visual inspection of the diffusion membrane at the end of the experiment revealed a bright purple coloration on the donor side, suggesting a partial Cy3 adsorption on it.

In the case of SLNs, CURC reveals a slow but continuous release, consistent with its lipophilic nature and gradual diffusion from the lipid core. In this work, CURC can be considered as a model to study the release of hydrophobic drugs from SLNs core and therefore its behavior exemplifies the release profile expected for other therapeutic molecules with similar lipophilic characteristics.
By contrast, Cy3 release from SLNs is extremely low (< 0.1%) and negligible over 24 hours, in contrast with the reference solution which displays around 40% membrane permeation within the same timeframe.

These results suggest that Cy3 is not released from the nanoparticles, but rather remains embedded within the SLNs as an integral part of the lipid matrix. This interpretation is consistent with the structural characteristics of Cy3, which contains two C8 alkyl chain that closely resemble triglycerides structure favoring its stable integration into the SLNs matrix.

5. CONCLUSIONS

The main aim of this work was to develop a reproducible, simple and cost-effective method to stably fluorescently label SLNs. The fluorophore needed to be incorporated within the lipid matrix to monitor the intracellular fate of the nanoparticle, rather than being encapsulated in the core like a drug payload.

Cy3 was synthetized through a simple procedure and its initial characterization displayed high brightness. The incorporation inside SLNs was successful and, after characterization, neither the dye nor the nanoparticles lost their physicochemical properties.

To better mimic a real SLNs delivery environment, CURC was co-entrapped with Cy3 in SLNs as a model drug, thus developing an embryonic theranostic system. The co-encapsulation could be confirmed by fluorescent microscopy analysis, since the same SLN could be visualized as bright spots either by exciting CURC or Cy3.

Additional studies have demonstrated the stable incorporation of Cy3 in the SLN matrix, as evidenced by its negligible release over 24 hours, in contrast to CURC which was gradually released as expected for a drug.

When co-encapsulated CURC and Cy3 form an efficient FRET pair. This feature can provide additional information on intracellular SLN fate. Cy3 fluorescence reports signal from the lipid matrix, while FRET signal reflects the proximity of CURC and Cy3, thus acting as a marker of SLNs integrity and drug release.

This work has therefore demonstrated the feasibility of stably labeling SLNs with a fluorophore, without the need for complex procedures, paving the way for future *in vitro* imaging studies. In particular, this system provides a platform for monitoring SLNs stability, intracellular nanoparticles fate and controlled drug release.

6. BIBLIOGRAPHY

1. Bertini, I. (ed.) (2009) *Inorganic and bio-inorganic chemistry*, Encyclopedia of life support systems ; Chemical sciences engineering and technology resources, Eolss Publishers, Oxford
2. Mishra, D., Hubenak, J. R., and Mathur, A. B. (2013) Nanoparticle systems as tools to improve drug delivery and therapeutic efficacy. *J Biomedical Materials Res*. **101**, 3646–3660
3. Romero, G., and Moya, S. E. (2012) Chapter 4 - Synthesis of Organic Nanoparticles. in *Frontiers of Nanoscience* (de la Fuente, J. M., and Grazu, V. eds), pp. 115–141, Nanobiotechnology, Elsevier, **4**, 115–141
4. H. Alshammari, B., A. Lashin, M. M., Adil Mahmood, M., S. Al-Mubaddel, F., Ilyas, N., Rahman, N., Sohail, M., Khan, A., Shukhratovich Abdullaev, S., and Khan, R. (2023) Organic and inorganic nanomaterials: fabrication, properties and applications. *RSC Advances*. **13**, 13735–13785
5. Musielak, E., Feliczak-Guzik, A., and Nowak, I. (2022) Synthesis and Potential Applications of Lipid Nanoparticles in Medicine. *Materials (Basel)*. **15**, 682
6. Gasco, M. R., Priano, L., and Zara, G. P. (2009) Solid lipid nanoparticles and microemulsions for drug delivery. in *Progress in Brain Research*, pp. 181–192, Elsevier, **180**, 181–192
7. Chirio, D., Peira, E., Dianzani, C., Muntoni, E., Gigliotti, C., Ferrara, B., Sapino, S., Chindamo, G., and Gallarate, M. (2019) Development of Solid Lipid Nanoparticles by Cold Dilution of Microemulsions: Curcumin Loading, Preliminary In Vitro Studies, and Biodistribution. *Nanomaterials*. **9**, 230
8. Harrington, K. J., Mohammadtaghi, S., Uster, P. S., Glass, D., Peters, A. M., Vile, R. G., and Stewart, J. S. (2001) Effective targeting of solid tumors in patients with locally advanced cancers by radiolabeled pegylated liposomes. *Clin Cancer Res*. **7**, 243–254
9. Calderón-Colón, X., Raimondi, G., Benkoski, J. J., and Patrone, J. B. (2015) Solid Lipid Nanoparticles (SLNs) for Intracellular Targeting Applications. *JoVE*. 10.3791/53102
10. Kristl, J., Plajnšek, K. T., Kreft, M. E., Janković, B., and Kocbek, P. (2013) Intracellular trafficking of solid lipid nanoparticles and their distribution between cells through tunneling nanotubes. *European Journal of Pharmaceutical Sciences*. **50**, 139–148

11. Bukhari, S. I., Imam, S. S., Ahmad, M. Z., Vuddanda, P. R., Alshehri, S., Mahdi, W. A., and Ahmad, J. (2021) Recent Progress in Lipid Nanoparticles for Cancer Theranostics: Opportunity and Challenges. *Pharmaceutics*. **13**, 840
12. Albuquerque, J., Moura, C., Sarmento, B., and Reis, S. (2015) Solid Lipid Nanoparticles: A Potential Multifunctional Approach towards Rheumatoid Arthritis Theranostics. *Molecules*. **20**, 11103–11118
13. 4.2: Cyanine Dyes (2013) *Chemistry LibreTexts*. [online] https://chem.libretexts.org/Bookshelves/Physical_and_Theoretical_Chemistry_Textbook_Maps/Book%3A_Quantum_States_of_Atoms_and_Molecules_(Zielinksi_et_al)/04%3A_Electronic_Spectroscopy_of_Cyanine_Dyes/4.02%3A_Cyanine_Dyes (Accessed August 20, 2025)
14. Lovell, T. C., Branchaud, B. P., and Jasti, R. (2024) An Organic Chemist's Guide to Fluorophores – Understanding Common and Newer Non-Planar Fluorescent Molecules for Biological Applications. *Eur J Org Chem*. **27**, e202301196
15. Annunziata, F., Pinna, C., Dallavalle, S., Tamborini, L., and Pinto, A. (2020) An Overview of Coumarin as a Versatile and Readily Accessible Scaffold with Broad-Ranging Biological Activities. *Int J Mol Sci*. **21**, 4618
16. Purr, E., Marshall, J., and Smith, J. (2019) Preparation of PLGA Nanoparticles Encapsulated with Fluorescent Probe Coumarin-6. 10.1101/614875
17. Brøndsted, F., and Stains, C. I. (2022) Heteroatom-Substituted Xanthene Fluorophores Enter the Shortwave-Infrared Region. *Photochem Photobiol*. **98**, 400–403
18. Li, F.-Z., Wu, Z., Lin, C., Wang, Q., and Kuang, G.-C. (2022) Photophysical properties regulation and applications of BODIPY-based derivatives with electron donor-acceptor system. *Results in Chemistry*. **4**, 100384
19. Trofymchuk, K., Valanciunaite, J., Andreiuk, B., Reisch, A., Collot, M., and Klymchenko, A. S. (2019) BODIPY-loaded polymer nanoparticles: chemical structure of cargo defines leakage from nanocarrier in living cells. *J. Mater. Chem. B*. **7**, 5199–5210
20. Comprehensive Overview of Cyanine Fluorophores: Structure, Applications, and Innovations in Fluorescent Labeling - Alfa Chemistry [online] https://www.alfa-chemistry.com/resources/comprehensive-overview-of-cyanine-fluorophores-structure-applications-and-innovations-in-fluorescent-labeling.html (Accessed August 24, 2025)
21. Mustroph, H. (2020) Cyanine dyes. *Physical Sciences Reviews*. **5**, 20190145

22. Van Der Wal, S., Kuil, J., Valentijn, A. R. P. M., and Van Leeuwen, F. W. B. (2016) Synthesis and systematic evaluation of symmetric sulfonated centrally C C bonded cyanine near-infrared dyes for protein labelling. *Dyes and Pigments*. **132**, 7–19
23. Chapman, G., Henary, M., and Patonay, G. (2011) The Effect of Varying Short-Chain Alkyl Substitution on the Molar Absorptivity and Quantum Yield of Cyanine Dyes. *Anal Chem Insights*. **6**, ACI.S6568
24. Ma, X., Huang, Y., Abedi, S. A. A., Kim, H., Davin, T. T. B., Liu, X., Yang, W.-C., Sun, Y., Liu, S. H., Yin, J., Yoon, J., and Yang, G.-F. (2022) Rational Design and Application of an Indolium-Derived Heptamethine Cyanine with Record-Long Second Near-Infrared Emission. *CCS Chem*. **4**, 1961–1976
25. Gorka, A. P., Nani, R. R., and Schnermann, M. J. (2015) Cyanine Polyene Reactivity: Scope and Biomedical Applications. *Org Biomol Chem*. **13**, 7584–7598
26. Sutton, P. A., van Dam, M. A., Cahill, R. A., Mieog, S., Polom, K., Vahrmeijer, A. L., and van der Vorst, J. (2023) Fluorescence-guided surgery: comprehensive review. *BJS Open*. **7**, zrad049
27. Pansare, V., Hejazi, S., Faenza, W., and Prud'homme, R. K. (2012) Review of Long-Wavelength Optical and NIR Imaging Materials: Contrast Agents, Fluorophores and Multifunctional Nano Carriers. *Chem Mater*. **24**, 812–827
28. Marcelo, G. A., Galhano, J., and Oliveira, E. (2023) Applications of cyanine-nanoparticle systems in science: Health and environmental perspectives. *Dyes and Pigments*. **208**, 110756
29. Carregal-Romero, S., Plaza-García, S., Piñol, R., Murillo, J. L., Ruiz-Cabello, J., Padro, D., Millán, A., and Ramos-Cabrer, P. (2018) MRI Study of the Influence of Surface Coating Aging on the In Vivo Biodistribution of Iron Oxide Nanoparticles. *Biosensors*. **8**, 127
30. Tiwary, P., Oswal, K., Varghese, R., and Gupta, P. (2026) Solid lipid nanoparticles in imaging, diagnostics and theranostics: A review of a decade of innovations and clinical applications. *Colloids and Surfaces B: Biointerfaces*. **257**, 115122
31. Pallares, R. M., Mottaghy, F. M., Schulz, V., Kiessling, F., and Lammers, T. (2022) Nanoparticle Diagnostics and Theranostics in the Clinic. *J Nucl Med*. **63**, 1802–1808
32. Williams, A. T. R., Winfield, S. A., and Miller, J. N. (1983) Relative fluorescence quantum yields using a computer-controlled luminescence spectrometer. *Analyst*. **108**, 1067

33. Pålsson, L.-O., and Monkman, A. P. (2002) Measurements of Solid-State Photoluminescence Quantum Yields of Films Using a Fluorimeter. *Adv. Mater.* **14**, 757
34. Quantum Yield [Rhodamine B] | AAT Bioquest [online] https://www.aatbio.com/resources/quantum-yield/rhodamine_b (Accessed September 5, 2025)
35. Williams, P. M. (2016) Zeta Potential. in *Encyclopedia of Membranes* (Drioli, E., and Giorno, L. eds), pp. 2063–2064, Springer Berlin Heidelberg, Berlin, Heidelberg, 10.1007/978-3-662-44324-8_612
36. Bajar, B. T., Wang, E. S., Zhang, S., Lin, M. Z., and Chu, J. (2016) A Guide to Fluorescent Protein FRET Pairs. *Sensors (Basel)*. **16**, 1488
37. Takakura, H., Sato, H., Nakajima, K., Suzuki, M., and Ogawa, M. (2021) In Vitro and In Vivo Cell Uptake of a Cell-Penetrating Peptide Conjugated with Fluorescent Dyes Having Different Chemical Properties. *Cancers*. **13**, 2245
38. Honig, M. G., and Hume, R. I. (1986) Fluorescent carbocyanine dyes allow living neurons of identified origin to be studied in long-term cultures. *The Journal of cell biology*. **103**, 171–187
39. Lee, H. K., Lee, D. J., Kim, H. M., Hwang, T. G., Kim, S., Kim, Y. S., Choi, W. J., Kim, W., Yoon, J. H., Jang, S. H., Lee, W., and Kim, J. P. (2025) Collaborative utilization of complementary cyanine dyes for application in broad-range NIR-absorbing films. *Progress in Organic Coatings*. **208**, 109436
40. Soriano, E., Holder, C., Levitz, A., and Henary, M. (2015) Benz[c,d]indolium-containing Monomethine Cyanine Dyes: Synthesis and Photophysical Properties. *Molecules*. **21**, 23
41. Maller, C., Schedel, F., and Köhn, M. (2024) A Modular Approach for the Synthesis of Diverse Heterobifunctional Cyanine Dyes. *J. Org. Chem.* **89**, 3844–3856
42. Zarow, A., and Shin, Y. (2009) Cyanine Dyes: Fine Structures in Their Absorption Spectra. *AJUR*. 10.33697/ajur.2009.009
43. Mustroph, H., Reiner, K., and Senns, B. (2017) Bond length alternation in unsymmetrical cyanine dyes and its influence on the vibrational structure of their electronic absorption spectra. *Coloration Technology*. **133**, 469–475
44. Cyanine3 NHS ester *Lumiprobe*. [online] https://www.lumiprobe.com/p/cy3-nhs-ester (Accessed August 13, 2025)

45. Muddana, H. S., Morgan, T. T., Adair, J. H., and Butler, P. J. (2009) Photophysics of Cy3-Encapsulated Calcium Phosphate Nanoparticles. *Nano Lett.* **9**, 1559–1566
46. Xu, M., Qi, Y., Liu, G., Song, Y., Jiang, X., and Du, B. (2023) Size-Dependent *In Vivo* Transport of Nanoparticles: Implications for Delivery, Targeting, and Clearance. *ACS Nano*. **17**, 20825–20849
47. Sousa De Almeida, M., Susnik, E., Drasler, B., Taladriz-Blanco, P., Petri-Fink, A., and Rothen-Rutishauser, B. (2021) Understanding nanoparticle endocytosis to improve targeting strategies in nanomedicine. *Chem. Soc. Rev.* **50**, 5397–5434
48. Ghosh, M., and Sarkar, N. (2024) Exploring the World of Curcumin: Photophysics, Photochemistry, and Applications in Nanoscience and Biology. *ChemBioChem*. **25**, e202400335